IMPROVING KNOWLEDGE OF PERMAFROST-AFFECTED SOILS IN ALASKA - FIELD DATA COLLECTION AND SAMPLING DESIGN TO SUPPORT CURRENT AND FUTURE SOIL SURVEY INITIATIVES

A Thesis

SUBMITTED TO THE FACULTY OF

UNIVERSITY OF MINNESOTA

BY

MICHAEL JOSEPH SOUSA

IN PARTIAL FULFILLMENT OF THE REQUIREMENTS

FOR THE DEGREE OF

MASTER OF SCIENCE

Dr. Nicolas Jelinski, Advisor

December 2020

ACKNOWLEDGEMENTS

I would like to thank my advisor, Dr. Nicolas Jelinski whose constant optimism and enthusiasm for scientific research motivated me to complete this degree. Dr Jelinski's guidance throughout this program has helped me achieve things I never thought possible within the academic and professional realm. I would not be where I am today without his support. Truly unmatched. I would also like to thank my committee members Jay Bell and Marcella Windmuller-Campione. A special thank you to Dr. Bell's guidance through my time as an undergraduate and graduate student and to Dr. Windmuller-Campione's unparalleled speed when meeting short notice manuscript submission deadlines. My thesis committee have been instrumental in the completion of my masters and my success overall as a student. I cannot thank them enough.

Additionally, I would like to thank Ahtna Incorporated and especially E. GreyBear and K. Finnesand for their help performing field work outlined in this text. Field work was also completed by A. Williams, V. Zachman, and many other to whom I am very grateful. I would also like to thank M.H. Clark, C.-L. Ping, and N. Parry for motivating discussions about Copper River Basin soils; and S. Bauer and K. Ring for assistance in the laboratory.

Lastly, I must thank my friends, fellow graduate students, and family. The moral support I have received has played a huge role in my success and I owe most of my work to the motivation instilled by these people.

ABSTRACT/SUMMARY

Lands in the United States without detailed soil survey coverage are considered "not complete" (NOTCOM). There are currently approximately 430 million acres of NOTCOM remaining in the United States, with Alaska making up more than 70% of this remaining area. The first part of this work is a collaborative sampling of black spruce forests and associated permafrost-affected soils in the central Copper River basin. After sampling sites under burned and unburned areas, we assess trajectories of soil carbon, permafrost and vegetation change following fire to inform future management strategies. The second portion of this work examined the utility of implementing a Conditioned Latin Hypercube Sampling (cLHS) methodology in order to locate optimal sampling locations for future study. The cLHS used in this study was constrained by an inclusive cost layer representing an aggregation of real-world costs associated with travel within the Yukon-Kuskokwim Delta study area located in south western Alaska.

TABLE OF CONTENTS

LIST OF TABLES

LIST OF FIGURES

CHAPTER 1 – LONG-TERM RECOVERY OF SOIL CARBON STOCKS AND PERMAFROST DEPTH LAGS RECOVERY OF ORGANIC LAYER THICKNESS FOLLOWING FIRE IN BLACK SPRUCE FORESTS OF THE COPPER RIVER BASIN, ALASKA

SYNOPSIS

This study investigated differences in forest structure, organic layer thickness, soil organic carbon, and permafrost depth between late successional (LS) and post fire (PF, 90 to 120 years since burn) plots under black spruce (Picea mariana (Mill.) BSP) on fine-textured, poorly drained lacustrine sediments in the Copper River Basin, Alaska. We found that although live stem and seedling density and organic layer thickness (OLT) was not significantly different between PF and LS plots (28 ± 7 cm and 31 ± 10 cm, respectively), soil organic carbon (SOC) stocks (30 ± 10 kg m^{-2} and 46 ± 12 kg m^{-2}, respectively), and permafrost depth (90 ± 28 cm and 56 ± 12 cm, respectively) remain significantly different. OLT was linearly related to 1 m SOC stocks for LS plots but not for PF plots, and LS plots had a greater proportion of highly decomposed (humic) material in the organic layer. Soil properties on PF plots appear to be on a trajectory of recovery towards LS plots with respect to SOC stocks, permafrost depth, and organic layer composition, but remain different despite nearly 100 years since fire disturbance and therefore potentially sensitive to changes in future fire frequency or climate.

INTRODUCTION

Boreal black spruce (Picea mariana (Mill.) Britton, Sterns & Poggenb.) forests are the most extensive forest type in the northern circumpolar zone of discontinuous permafrost and are large reservoirs of soil carbon (Dyrness and Norum, 1983; Genet et al., 2013). This is especially true in the Copper River basin (CRB) ecoregion of Alaska (Gallant et al., 1995, Nowacki et al., 2001) where black spruce forests account for nearly 38% of the land area (LANDFIRE, 2017). Fire plays an integral role in the ecology of black spruce forests in Alaska through its impacts on both aboveground vegetation and soil characteristics (Kasischke and Johnstone, 2005). In particular, fire frequency and severity affects the thickness of the insulating surface organic materials (organic layer thickness, or OLT), a critical soil characteristic that is tightly linked to permafrost dynamics and soil organic carbon (SOC) stocks (Kasischke et al., 2000; O'Donnell et al., 2011; Fisher et al., 2016; Minsley et al., 2016). Under natural fire regimes, there is evidence for a cyclical pattern of fire, permafrost recession and SOC loss, followed by permafrost aggradation and SOC gain following recovery of OLT (Viereck, 1970, 1983a; Yi et al., 2009a, 2009b).

Projections suggest both climate-driven permafrost degradation (Pastick et al., 2015; 2017) and increases in fire frequency (Kasischke et al., 2010) throughout the 21st century which, in concert, have the potential to impact SOC stocks under black spruce forests by

changing the rate of OLT and permafrost recovery after fire (Genet et al., 2013; Minsley et al., 2016). Understanding the sensitivity of carbon dynamics under black spruce forests to fire is therefore critical for effectively predicting and modeling the response of boreal soil carbon (O'Donnell et al., 2011). Due to difficulties in assessing the long-term (decadal to century-scale) responses of OLT recovery, SOC stocks, and active layer thickness at a single plot, many studies have utilized a space-for-time approach to assess these trajectories, comparing burned and unburned forests with known time intervals since fire disturbance (O'Donnell et al., 2011; Turetsky et al., 2011; Hoy et al., 2016).

Notably, the majority of these space-for-time studies have focused on black spruce forests of the Alaskan interior, north of the Alaska Range (Turetsky et al., 2011; O'Donnell et al., 2011; Minsley et al., 2016), while comparatively little data are available from the CRB (Ping et al., 2010; Jelinski et al., 2019). Studies in the discontinuous permafrost zone in interior Alaska have estimated pre-industrial fire return intervals of 35-200 years (Johnson, 1979; Heinsleman, 1981; Yarie, 1981; Hu et al., 2006), while pre-industrial fire return intervals in the CRB were likely longer (150 to > 500 yr), largely due to decreased incidence of lightning (Lynch et al., 2004; Hu et al., 2006; Fryer, 2014). Additionally, soils under black spruce in the CRB (a large, intermontane basin repeatedly occupied by proglacial lakes during the Pleistocene) are predominantly formed in clayey glaciolacustrine sediments on flat landscapes and poorly

to very poorly drained (Ping et al., 2004; O'Donnell et al., 2010; Jelinski et al., 2019). Thus, the differences in ecological conditions in the CRB could have major impacts on post-fire ecosystem recovery over long timescales.

Soil texture has been shown to interact with other site variables to influence aboveground biomass production and SOC stocks in boreal forests (Bhatti and Apps, 2000; Bhatti et al., 2002), and trajectories of soil recovery under black spruce can be strongly influenced by both soil texture and topographic position (Houle et al., 2018). In particular, over the short term (decadal scale), fine-textured soils may experience faster recovery and accumulation of less dense, more fibric organic materials following fire disturbance than coarse-textured, better drained sites (Houle et al., 2018). Given that the permafrost-affected soils under black spruce in the CRB are generally fine-textured (30-64%) clay (Jelinski et al., 2019)), and that fine-textured glaciolacustrine parent materials are undersampled in Alaska generally (Ping et al., 2010), the CRB represents an important opportunity to add to the body of knowledge of permafrost-affected soil properties under black spruce and their response over time following disturbance.

The objectives of this work were to use a space-for-time approach to conduct a comparative analysis of the above and belowground characteristics of late successional (LS) and post fire (PF) black spruce stands overlying permafrost in the Copper River Basin in order to better characterize the differences in and apparent recovery trajectories

of (i) forest structure, (ii) thickness of the soil organic layer and depths to permafrost, (iii) organic layer decomposition states, and (iv) SOC stocks, approximately one century following a large stand-replacing fire event.

MATERIALS AND METHODS

Study Area

The Copper River Basin (CRB) is an intermontane basin in south-central Alaska bounded by the Alaska and Chugach Ranges on the north and south, and Talkeetna and Wrangell mountains on the west and east, respectively. (Nowacki et al., 2001; Soil Survey Staff, 2006) The basin was repeatedly occupied by proglacial lakes throughout the Pleistocene, which formed due to the damming of the southern outlet of the basin by mountain glaciers (Bennett et al., 2012). Final drainage of the most recent lake is presumed to have occurred approximately 9,000 yBP. (Ferrians et al., 1983). Soil parent materials in the central part of the basin are dominated by calcareous, clayey, glaciolacustrine sediments overlain in some areas by a thin loess cap which increases dramatically in thickness from north to south (Clark and Kautz, 1990, 1999; Muhs et al., 2013; Jelinski et al., 2019). Elevations in the basin range from 170m asl in the incised drainages of the Copper River (Figure 1) to 1100m asl in the outer uplands surrounding the basin rim (Ping et al., 2004). Mean annual precipitation in the central part of the CRB near the study area (Gulkana, AK) between 1981-2010 was approximately 280 mm, while mean annual air temperature for the same was 2.1°C (WRCC, 2019).

The most extensive forest communities in the central part of the CRB are *P. mariana* (black spruce) dominated forests on the permafrost-affected soils of poorly

drained clayey uplands (Clark and Kautz, 1999). These communities have been characterized as spruce-muskeg sedge open forests or spruce/water sedge woodlands (Clark and Kautz, 1999), and experience fire on return intervals of approximately 150 to 500 years (Lynch et al., 2004; Fryer et al., 2014). Using the black spruce forest community classification schemes of Nettleton-Hollingsworth (2004), the LS black spruce forests in our study area are best characterized as acidic, wet, black spruce forests, while adjacent burned areas tend towards non-acidic, wet, black spruce forest community types. Common species in the shrub stratum include *Arctostaphyos rubra, Betula glandulosa, Empetrum nigrum, Rhododendron groenlandicum, Salix* spp*., Vaccinium uliginosum, and Vaccinium vitis-idea* (Clark and Kautz, 1999, Table 3). Sedge (*Carex lugens, Carex aquatilis*) and graminoid (*Arctagrostis latifolia, Calamagrostis canadensis*) species are common, along with forbs such as *Petasites frigidus, Equisetum* spp., and *Rubus chamaemorus* (Clark and Kautz, 1999, Table 3). Presence-absence data indicates that a few key shrub, forb and bryophyte species (*Aulocomium* spp., *Equisetum palustre*, *Polygonum alpinum*, and *Rosa acicularis*) may be understory indicators of past fire disturbance (Table 3)

Study Plot Selection

In late August of 2017 and 2018 (close to the timing of maximum thaw depth – Dyrness, 1982), we examined a total of 44 plots in 9 distinct clusters (3 clusters of plots

in LS stands and 6 clusters of plots in PF stands) in the central CRB (Figure 1). Of these 44 plots, half (n = 22) were located in LS black spruce stands, and half (n = 22) were located in PF black spruce stands. Although the entire CRB has experienced fire at return intervals on the order of centuries (Lynch et al., 2004), we attempted to select mature, LS black spruce-dominated plot locations in our study area to pair them with adjacent PF black spruce plots that showed evidence of a historic stand replacing fire. PF plot selection was performed using a combination of satellite imagery and on-the-ground observational data of tree stand density, growth habit, distribution of tree heights, and observations of fire scars on standing dead or live trees. The effects of historic fire disturbance at these plots was still clearly visible during our fieldwork and was confirmed by tree ring counts taken during this study. Given patterns in vegetation from satellite imagery, tree ring count data, and local generational knowledge (K. Linnell, Ahtna Intertribal Resource Commission, personal communication), one or multiple fire events occurred at all PF plots in our study area between 1897 and 1929 CE. Because the Alaska Large Fire Database (AICC, 2018) only contains fire perimeters since 1942 CE and fire locations since 1939 CE, the exact year and full extent of these fires is unknown. However, using the method of Kasischke and Johnstone (2005), we estimated minimum stand age or time since burn for each cluster of plots. Following Kasischke and Johnstone (2005), the ring counts of the oldest trees in each plot were used and trees were assumed to have grown for 5 years prior to reaching the sampling height (see section 2.3, below).

These resulted in time since burn estimates for the PF plots of approximately 89 ± 4 years (1929 CE, n = 17) or 121 ± 6 years (1897 CE, n = 5) prior to our sampling. Using the same method for the LS plot clusters resulted in stand initiation or time since burn estimates of 174 ± 10 (1843 CE, n = 8), 215 ± 12 (1802 CE, n = 8), and 229 ± 42 years (1788 CE, n = 6). The soils and landscapes sampled as a part of this project are part of the Native Territory of the Ahtna people.

Forest Inventory

Fixed radius circular 0.004 ha plots were established at each of the 22 LS and 22 PF plots to measure non seedling trees. Non seedling trees were defined as any tree species with a diameter at breast height (dbh, 1.3 m) greater than 2.54 cm. Forest inventory variables were recorded for all trees within each plot, including status (live or dead), species, dbh, and height. These same plot boundaries were used to measure seedling densities by species; seedlings were defined as any tree species with a dbh less than 2.54 cm. Understory plants (shrubs, herbaceous plants, and lichens) were recorded using the relevé method within each plot boundary, recording species presence but without estimates of areal coverage (Jennings et al., 2004).

At each plot, starting due north from the plot center, the first three trees encountered were sampled to determine ring counts either by collecting tree stem disks or by increment borer. Sampling occurred approximately 10-15 cm above the soil surface,

avoiding any swollen portions of the stem base. Cores and cookies were sanded using progressively finer grits (120-420) to expose the yearly growth rings. Each core was dotted using a standard decadal dotting system (4 dots for a millennium, 3 every century, 2 every 50 years, and one every decade). Growth rings in the cores and cookies were then counted using a Velmex (Velmex INC 2009) data recorder and binocular microscope.

Soil Sampling and Sample Preparation

At each plot an approximately 0.5 m diameter soil profile was excavated to the bottom of the active layer, or to a depth of 1 m, whichever was shallower. When the soil could be excavated to the bottom of the active layer, a SIPRE (Snow, Ice, and Permafrost Research Establishment) corer (Rand and Mellor, 1985) was used to sample frozen soil materials to a depth determined by length of coring equipment or auger refusal by coarse fragments. It is important to note that because we do not have any pre-burn observations for our investigated plots, differences in estimates of depth to permafrost presented in this study are relative and not absolute, because we could not account for changes in absolute surface elevation following fire disturbance. In cases where absolute elevation of the ground surface decreased following fire due to permafrost recession or collapse of the organic layer, our estimates of differences between LS and PF plots would be conservative, and the absolute amount of permafrost recession experienced on PF plots could be much greater.

For plots where unfrozen soil material existed below a depth of 1 m, a manual bucket auger was used to extract deeper materials. Soil morphology (color, texture, structure, coarse fragments) and genetic horizons observed in the active layer were described in the field. The thicknesses of materials in the soil organic layer were determined using both the Canadian System of Soil Taxonomy (CSSC, Soil Classification Working Group, 1998) and U.S. Soil Taxonomy (Soil Survey Staff, 2014) guidelines. In the Canadian system, organic horizons (O horizons) comprised of peat materials are categorized as fibric (Of, > 40% rubbed fiber content), mesic (Om, 10 to 40% rubbed fiber content), and humic (Oh, < 10% rubbed fiber content) materials, which are broadly equivalent to fibric (Oi), hemic (Oe) and sapric (Oa) organic material definitions in U.S. Soil Taxonomy. Soils investigated at all 44 plots were classified as Cryosols (CSSC, Soil Classification Working Group, 1998) or Gelisols (U.S. Soil Taxonomy, Soil Survey Staff, 2014). Of these 44 soils, 5 (11%) were Organic Cryosols (CSSC) or Histels (U.S. Soil Taxonomy) and 39 (89%) classified as Turbic Cryosols (CSSC) or Turbels (U.S. Soil Taxonomy).

Soil bulk density samples were collected using standardized methodologies for permafrost-affected soils, depending on thermal state and material type (Ping et al., 2013). As it is inappropriate to use the clod or ring methods on organic materials, surface organic horizon bulk densities were collected using a serrated knife to cut precision cut

blocks of approximately 250 cm^3 (5 cm x 5 cm x 10 cm) from the pit face. For horizons that were too thin to be sampled using this standardized size, blocks were cut and dimensions measured to the nearest cm to determine volume in the field. Unfrozen mineral soil samples were collected using the ring method, attached to a short slide hammer (Soil Moisture Inc) using a core of known volume with beveled edges. A SIPRE corer (76 mm inner diameter) was used to recover cylindrical samples of known length from frozen materials below the active layer. These cores were described in the field, following standardized conventions for horizon nomenclature and soil morphological properties (Schoeneberger et al., 2011), and sampled by segmenting subsections of the core corresponding to genetic horizons with a Craftsman 12v multi-tool. All frozen samples were quickly sealed in plastic bags to prevent water loss (Michaelson et al., 1996; Ping et al., 2013).

A total of 412 (220 LS and 192 PF) physical soil samples were collected in the field. Samples were then dried in the laboratory at 60°C, hand ground with a mortar and pestle, and sieved to separate fine earth (< 2 mm) from coarse fragments and large pieces of organic material (>2 mm). After sieving, the fine earth fraction was used to characterize pH, loss on ignition, soil organic carbon (SOC), field water content, and bulk density. Coarse fragments (particles >2 mm) that did not pass through the sieve were retained, shaken overnight in a Na-hexametaphosphate and deionized water solution to

remove any adhering soil particles, oven dried for 24 hours at 105°C, and weighed. Coarse fragments, on average, accounted for < 1% of the bulk mass of any particular physical sample taken from the field. On the same day that physical and chemical characterization of fine earth (< 2 mm) was initiated, a sub-sample of the air-dried material was placed in a drying oven for 24 hr. at 105 ºC and weighed prior to and after drying in order to account for the moisture content of the air-dried sample used for analysis. Thus, the bulk densities reported, and all other proportions of soil constituents reported in the data represent percentages of oven-dried fine-earth (< 2 mm) material. Gravimetric water content (θ_g, including solid and liquid phases) for each sample was determined by the difference between the field moist mass of the bulk sample (weighed within 8 hours of collection in the field) and the oven dry mass of the bulk sample (obtained by applying a moisture correction to the bulk mass of the air-dried samples after drying a subsample at 105 ºC for 24 hr.).

2.5 Soil pH, Soil Organic Carbon Concentrations, Bulk Densities, and Soil Organic Carbon Stocks

Soil pH for mineral samples was determined in 1:1 slurry of 5g of air-dried soil and 5ml of water (pH_{H2O}). For organic soil samples, a 2:1 soil-water slurry was utilized

because a 1:1 slurry for organics does not typically produce enough free water once added to dry organics to produce a reliable slurry and pH measurement. All samples were analyzed for loss on ignition (LOI, weight %) at 550° C for 5 hr and predicted SOC concentration was determined by utilizing a previously developed regression of SOC determined by dry combustion to LOI for soils of the CRB ((Jelinski et al., 2019), SOC = 0.538*LOI – 0.816; $R^2 = 0.994$, $p < 0.001$, n = 136). Whole profile carbon stocks were calculated to a depth of 1 m on an aerial basis as

$$Profile\ SOC\ Stock\ (1m)\ kg\ m^{-2} =$$

$$\sum_{i=1}^{n} SOC\ concentration\ (kg\ kg^{-1})\ x\ \rho_b (kg\ m^{-3})\ x\ h(m) \qquad (1),$$

where n is the number of soil horizons to 1 m depth, ρ_b is the coarse-fragment free soil bulk density, and h is thickness of each soil horizon. In addition to whole profile carbon stocks, depth-normalized carbon density calculations (carbon stock per cm depth) were calculated for each soil horizon as

$$Depth\ Normalized\ Carbon\ Density\ (kg \cdot m^{-2} \cdot cm^{-1}) = \frac{Horizon\ SOC\ stock\ (kg\ m^{-2})}{Horizon\ thickness\ (cm)}$$

(2),

where horizon thickness is expressed in cm and is the difference between lower horizon boundary and top horizon boundary of the soil genetic horizon.

2.6 Data Analysis

All statistical data analyses were performed in R (version 3.6.1, R Core Team, 2019). Although the PF plots were clearly differentiated from the LS plots with regard to time since disturbance or stand initiation (average difference of 112 yr), it is possible our PF plots may have been burned in two different events (17 plots with an estimated burn year of 1929 ± 4 CE and 5 plots with an estimated burn year of 1897 ± 6 CE). Additionally, the estimated average ages of the LS plots varied by approximately 50 years (174 to 229 yr). We therefore analyzed the data using two distinct approaches. In the first approach, we treated all PF plots as a group and all LS plots as a group and tested for differences between forestry and soil metrics using Welch's two-sample t-test for group means (Welch, 1947). In the second approach, we calculated averages of stand age

and forestry and soil metrics by plot clusters (n = 9) and utilized linear and non-linear regression to investigate potential trends in these metrics over time since disturbance or stand initiation. The linear models were used to derive average values of change over time, but we interpret the results of these models only within the range of our stand age data, because trajectories of SOC accumulation, tree size, and permafrost depth are typically highly non-linear over long timescales (Kasischke and Johnstone 2005, O'Donnell et al., 2011, Minsley et al., 2016, Pastick et al., 2017).

Unless otherwise mentioned in manuscript text or figure captions, all reported uncertainties represent a single standard deviation around the mean. Because our soil samples were collected on the basis of genetic horizons described in the field, we calculated the weighted averages of all available soil properties by depth increment for each sampling plots using the "slab" function in the Algorithms for Quantitative Pedology (AQP) package in R (Beaudette et al., 2013; R Core Team, 2016). Across all sampling plots, pH, gravimetric water content, bulk density, and normalized carbon density values were slabbed to standardized depth increments of 0 – 20 cm, 20 – 50 cm, and 50 – 100 cm in AQP. These standardized depth-increment weighted averages were utilized to compare the differences between soil properties with depth between LS and PF plots. The AQP package was also utilized to generate mean values and uncertainties for continuous depth functions (1 cm averages) of soil properties.

RESULTS & DISCUSSION

Comparison of Forestry Metrics Between LS and PF Plots

Over 98% of the trees (dbh > 2.54 cm) observed across all plots investigated were black spruce, while the remaining trees were white spruce (Picea glauca (Moench) Voss). Tree density was highly variable and not significantly different between LS and PF plots ($p = 0.5$), with LS stem densities averaging 3,047 ± 1,386 stems ha-1 and PF stem densities averaging 3,380 ± 1,621 stems ha-1 (Table 1). Seedling density was also not significantly different between the LS and PF plots ($p = 0.4$), with approximately 6,238 ± 3,279 seedlings ha-1 on LS plots and 7,050 ± 2,929 stems ha-1 on PF plots (Table 1). There was no significant influence of stand age on either seedling density or tree density ($p > 0.99$ and $p > 0.88$, respectively).

Tree dbh was significantly greater on LS plots (6.5 ± 1.8 cm) than PF plots (4.5 ± 1.0 cm, $p < 0.001$, Table 1); and trees on LS plots were also significantly taller (5.4 ± 2.1 m) than trees on PF plots (3.4 ± 1.3 m) ($p < 0.001$, Table 1). There was no significant relationship between tree age and top height when trees in LS ($p = 0.21$) or PF ($p = 0.79$) stands were analyzed independently, however there was a significant relationship between tree age and height when all trees (from both LS and PF plots) were included in the model ($R2 = 0.27$, $p < 0.001$). Both dbh ($R2 = 0.43$, $p = 0.032$) and tree height ($R2 =$

0.51, p = 0.018) averages by plot cluster increased significantly as stand age increased (Figure 2), with dbh increasing on average by 0.18 cm yr-1 and height increasing by 1.5 cm yr-1 (Figure 2). Ring count data from tree cores and cookies resulted in age estimates for black spruce trees growing on LS plots ranging from 132 to 264 yr with an average of 206 ± 29 yr (Figure 2). In contrast, black spruce trees growing on PF plots were significantly younger ($p < 0.001$, Table 1), ranging in age between 83 and 130 yr with an average age of 94 ± 14 yr. The ring count distribution for sampled trees on PF plots showed a unimodal age distribution indicative of even-aged stands, while the LS plots have a wider age class distribution with multiple recruitment periods common of multi-aged stands.

Organic Layer Thickness, Composition, and Relationships with Depth to Permafrost

A total of 126 organic soil horizons were described in the field, 60 (48%) of which were described as humic (Oh, Canadian Soil Classification System) 22 (17%) as mesic (Om, Canadian Soil Classification System), and 44 (35%) as fibric (Of, Canadian Soil Classification System). Organic layer thickness (OLT) on PF plots was not significantly different from OLT in LS plots (25.6 ± 7.4 cm and 30.4 ± 10.5 cm, respectively, Table 1, p = 0.08), and similarly no significant trend in increasing average OLT with average stand age by cluster was observed (p = 0.07).

However, despite similar total OLTs, LS plots consistently had significantly thicker, more decomposed, humic (Oh) horizons (16.7 ± 9.9 cm) and significantly thinner, less decomposed, fibric (Of) horizons (10.5 ± 4.3 cm) relative to PF plots (10.5 ± 5.2 cm and 12.2 ± 3.3 cm for Oh and Of horizon designations respectively, Table 1). Trends in average thicknesses of fibric (Of, $R2 = 0.41$, $p = 0.038$) and humic (Oh, $R2 = 0.59$, $p < 0.01$) materials by stand age were consistent with comparisons among all LS and PF plots. The proportional thickness of fibric materials within the organic layer decreased by approximately 0.1%/yr ($R2 = 0.72$, $p < 0.01$) (Figure 3a), while the proportional thickness of humic materials increased by approximately 0.1%/yr ($R2 = 0.46$, $p = 0.027$) (Figure 3b).

Depth to permafrost was significantly deeper under PF plots (89.5 ± 27.0 cm) than LS plots (55.6 ± 11.9 cm) ($p < 0.001$, Table 1, Figure 4) and while OLT was linearly related to depth to permafrost on LS plots ($R2 = 0.31$, $p < 0.001$, Figure 4) this relationship was not significant for PF plots ($p > 0.01$, Figure 4). Depth to permafrost decreased with stand age by an average of -0.26 cm per year ($R2 = 0.65$, $p < 0.01$, Figure 5a). Multiple linear regression found no other significant predictor variables for depth to permafrost for either PF or LS plots after OLT was incorporated into the model.

Depth Trends in Soil pH, Water Content, Bulk Density, and Horizon Normalized Carbon Density

Average soil pH across all standardized depth increments was significantly higher on PF plots than LS plots (6.7 ± 0.3 and 6.1 ±0.2, $p < 0.001$, Table 2) respectively. Soil pH under both LS and PF plots was lowest in surface organic materials (Figure 6a), and abruptly increased to an average of 5.6 for LS and 6.2 for PF at 10 to 20 cm (Figure 6a). After sharp increases at both LS and PF plots at the interface of the organic layer and mineral soil materials, pH steadily increased with depth. Average gravimetric water content (□g) at the time of sampling was highest in the surficial organic materials (Figure 6b), and abruptly declined to a minimum of 46% at 55 cm for PF plots and 55% at 51 cm for LS plots. PF plots were generally observed to be wetter than LS plots, which is reflected in the higher water contents of the upper organic materials at PF plots (312.9 g H2O g soil-1) relative to LS plots (214.1 g H2O g soil-1).

Bulk density was lowest in the surficial organic materials and increased rapidly through the upper mineral soil materials to a maximum of 1.1 g cm-3 for both LS and PF plots at approximately 50 cm (Figure 6c). Trends in depth-normalized carbon density (Equation 2) varied significantly ($p < 0.01$) between LS and PF plots. Large increases of normalized carbon density were observed in the lower organics on LS plots (Table 2, Figure 6d), associated with humic materials. These large increases in normalized carbon density were not observed in PF plots (Figure 6d), which had a larger proportion of fibric materials in

the lower organic layer. Although depth-normalized carbon densities were greater on LS plots than PF plots at all depth intervals (0-20 cm, 20-50 cm, and 50-100 cm), these differences were greatest in the 0-20 cm depth increment (0.79 ± 0.29 kg m-2 cm-1 and 0.31 ± 0.10 kg m-2 cm-1) for LS and PF plots, respectively, $p < 0.01$, Table 2).

Soil Organic Carbon Stocks and Carbon Stock Partitioning

Across all 44 plots SOC stocks to 1 m ranged from 15 to 68 kg m-2 with an average of 38 ± 14 kg m-2. Although large ranges in SOC stocks were observed for both LS and PF plots, total SOC stocks to 1 m depth at LS plots (25 to 68 kg m-2, average of 46 ± 12 kg m-2) were significantly greater than 1 m SOC stocks at PF plots (15 to 49 kg m-2, average of 30 ± 10 kg m-2) ($p < 0.01$, Table 2). On average, across both PF and LS plots, 48 ± 17% of the total 1 m SOC stock was contained in the organic layer (Table 2). Notable differences were observed between the proportion of 1 m SOC stocks contained in the organic layer between LS and PF plots. The proportion of SOC stocks contained in the organic layer at LS plots ranged from 33 to 91% and averaged 56 ± 14%, while for PF plots the proportion ranged from 20 to 72% and averaged 39 ± 15%. OLT was positively correlated with SOC stocks for LS plots (Figure 7, $R2 = 0.48$, $p < .001$) but not PF plots (Figure 7, $p = 0.07$). Stand age was significantly related to 1 m SOC stocks, with increasing SOC stocks associated with increasing stand age (average of 0.14 kg C m2 yr-1, $R2 = 0.48$, $p = 0.023$, Figure 5b).

Differences in Forest Structure and Age Between Late Successional and Post Fire Black Spruce Plots

PF plots investigated in this study had a uni-modal tree age distribution, common of even-aged stands that are transitioning between stand initiation and stem exclusion, as compared to the wider age class distribution of the LS plots which may be more representative of old-growth or multi-aged complex (Oliver and Larson, 1996; Franklin et al., 2002). Higher tree densities than those reported here were observed in other studies in interior Alaska (4,153 □ 472 stems ha-1 (acidic), 5,133 □ 516 stems ha-1 (non-acidic type), (Hollingsworth, 2004, near Fairbanks, AK) and 4,892 to 7,188 stems ha-1 (nonacidic, wet and dry), (Kasischke and Johnstone, 2005, near Delta Junction, AK). The lower stem densities reported in the LS and PF plots investigated in the CRB in this study may be due to the fact that these stands are borderline acidic (mineral soil pH between 4.9 and 6.0) and quite wet (poorly to very poorly drained soils), in contrast to the more mesic sites investigated in Hollingsworth (2004) and non-acidic sites investigated in Kasischke and Johnstone (2005). Thus, both hydrology and pH, and other factors such as competition may be important in controlling the stand densities reported here (Kasischke et al., 2000). Additionally, results from the Boreal Forest Transect Case Study (BFTCS, Bhatti and Apps, 2000) show that aboveground tree biomass decreased with increasing clay content on poorly drained sites. Therefore, the high clay contents of the soils

developed on glaciolacustrine sediments in the CRB (Jelinski et al., 2019) could also be contributing to the lower stem densities on the sites investigated in this study.

While both stem density and seedling densities did not differ between LS and PF plots, black spruce trees at LS plots had significantly greater diameters (dbh) and heights when compared to PF plots. Tree heights (3.4 ± 1.3 m) and diameters (4.5 ± 1.0 cm) on PF plots reported in this study were lower than those reported in Nettleton-Hollingsworth (2004) (4.1 to 4.8 m in mesic to xeric non-acidic and acidic sites in the Alaskan interior, and 5.0 to 5.5 cm dbh), but trees on LS plots were taller (5.4 ± 2.1 m), with larger dbh (6.5 ± 1.8 cm). For both LS and PF plots, there was no significant relationship between tree height and age; many of the trees at both sites index values that were below 5 (Rosner, 2004). Although temporal trends in stand development likely account for the larger trees on LS plots, persistent changes to edaphic factors even nearly a century after fire disturbance may play a role as well. PF plots had greater depths to permafrost and higher soil pH values than LS plots but were also wetter – this is in contrast to other studies in black spruce forests with underlying permafrost (Jorgenson and Osterkamp, 2005; Sniderhan and Baltzer, 2016) which have attributed poor growth following permafrost recession to drought stress. On the flat, poorly drained landscapes and fine-textured soils of the CRB, it is unlikely that drought stress plays a major role in tree growth trends. Instead, PF plots were observed to be wetter and slightly lower in

elevation than adjacent LS plots, perhaps due to elevation changes following fire and permafrost recession that have been further reinforced by localized hydrologic changes.

OLT and Depth to Permafrost Under Black Spruce in the CRB

Soil organic layer thickness and decomposition state are critical site variables (O'Donnell et al., 2009; Fisher et al., 2016) that impact soil temperature and moisture and thus, in turn, affect permafrost temperature and stability (Viereck 1983b; O'Donnell, 2011; Fisher et al., 2016; Minsley et al., 2016). The OLT values observed in this study are on the high end (12.0 cm to 48.0 cm) of the ranges of OLT reported from other sites under black spruce in interior Alaska (2.5 to 33 cm, Kasishcke and Johnstone, 2005; 3.0 to 39 cm, Ping et al., 2010).

Despite the fact that OLT was not significantly different between LS and PF plots, differences did exist in the degree of decomposition of organic materials and in depth to permafrost. LS plots had significantly more highly decomposed, humic, materials in the organic layer (Table 1), while PF plots had, on average, a greater proportion of fibric materials, suggesting that, in the absence of recent fire, organic layers under LS plots are older and more humified. This is supported by our analyses of Oh thicknesses with stand age (Figure 3), which show the apparent trajectories of increasing proportions of humic

materials at the expense of fibric materials over time. The presence of greater proportions of less decomposed materials on PF plots suggests that highly decomposed organic layers that were possibly once present were partially, or completely, collapsed and/or removed by fire and have been replaced by less decomposed fibric materials as these sites have recovered over the past century. A number of studies in boreal forest systems have shown that slow burning ground fires in boreal forests can remove a significant amount of deep organic materials. This is especially apparent in forests growing over permafrost affected soils (Dyrness and Norum, 1983; Landhausser and Wein 1993; Kasischke et al., 2000; Miyanishi and Johnson 2003).

The absence of a relationship between OLT and depth to permafrost in PF plots could be a signal of delayed permafrost aggradation. Disturbances such as fire that remove or collapse portions of the soil organic layer can result in permafrost degradation proportional to the amount of organic material lost (Dyrness, 1982). One plausible explanation for these observations could be changes to local site hydrology following fire, OLT reduction, and permafrost degradation. The combination of higher thermal conductivity in poorly drained organic materials (O'Donnell et al., 2009) and increased local subsurface flow to burned areas from higher elevation unburned areas and could slow permafrost recovery times. Previous observations have shown that the permafrost table may recede more than 50 cm to 1 m following fire in black spruce forests of the

CRB (Clark and Kautz, 1999). While subsidence or a collapsing ground surface may tend to reduce our estimates of absolute differences in changes to depth to permafrost between LS and PF sites, our data shows that even after nearly a century of recovery, the permafrost table at PF plots remains significantly deeper on average than at LS plots.

Soil Organic Carbon Stocks, Stock Partitioning, and Organic Layer Composition

The 1 m SOC stocks reported for the 22 LS plots investigated in this study are generally within the range of those reported for poorly drained to very poorly drained soils under black spruce throughout the Alaskan interior (Ping et al., 2010), which averaged 46 kg SOC m-2 (n = 19) and 51 kg SOC m−2 (n = 6), respectively. These 1 m SOC stocks are relatively high in the context of SOC stocks across the state of Alaska for non-peatlands (Johnson et al., 2011) and are much higher than 1 m SOC stocks reported in larch (Larix laricina (Du Roi) K. Koch) -dominated forests in Siberia (11 kg SOC m−2) (Webb et al., 2017), well drained to moderately well drained soils under black spruce formed in loess in interior Alaska (average, 17.1 kg SOC m−2) (O'Donnell et al., 2011), and previously SOC stocks reported for a single site under black spruce in the southern CRB (20.7 kg SOC m−2) (Ping et al., 2010). The percentage of 1 m SOC stocks contained in organic materials in this study differed significantly between PF (39%) and LS spruce plots (56%). These values for LS spruce plots were generally in line with poorly drained and

very poorly drained sites reported in statewide meta-analysis (57%) (Ping et al., 2010). Our analysis of SOC stocks by apparent stand age indicates that PF plots may still be on a trajectory that is accumulating SOC (Fig 7d), however it is likely that SOC accumulation rates are non-linear over longer time periods (Zhuang et al., 2003, Houle et al., 2018).

It appears that, a century after fire, organic layer composition, and not absolute OLT is the major driver of SOC stocks to 1 m. Depth-normalized carbon densities in lower portions of surficial organics (0-20 cm) were significantly higher on LS plots compared to PF plots. Thicker, more highly decomposed humic (Oh) materials on LS plots had higher carbon densities than newly formed less decomposed fibric (Of) organic material of PF plots, leading to greater 1 m SOC stocks at LS plots, despite the fact that OLT does not differ between LS and PF plots. This explains why OLT was a good predictor of SOC stocks in LS spruce plots but not in PF plots. In addition to total OLT, therefore, the degree of decomposition of organic materials is a critical factor in determining SOC stocks, as both carbon concentration and bulk density increase with increasing decomposition (Jelinski et al., 2019).

CONCLUSIONS

Our results show that despite major differences in tree size in LS and PF black spruce stands on permafrost-affected soils in the CRB approximately one century following fire disturbance, total OLT has largely recovered. It is also clear that for these sites on the

poorly drained, fine-textured glaciolacustrine sediments of the CRB, OLT is only a partial metric of site recovery. SOC stocks to 1 m on PF plots continue to lag OLT recovery because of the larger proportion of fibric material relative to humic material in the organic layer under PF stands. In addition, permafrost aggradation also appears to lag OLT recovery, as depth to permafrost under PF stands was significantly deeper even though OLT was similar to LS stands. Analysis of trends in soil properties by stand age suggests that depth to permafrost, organic layer composition, and SOC stocks are still on a trajectory towards recovery in the next 100 years on PF plots. However, the complex relationships between OLT, SOC stocks and permafrost depth coupled with a projected increase in fire frequency suggest that the trajectory of these soils may be sensitive to ecological change. Given that total OLT and organic layer composition are major drivers of SOC stocks to 1 m, suppression of the formation of more highly decomposed organic materials over time by increasingly frequent fire regimes could decrease SOC stocks in the long term. With projected long-term increases in fire frequency (Kasischke and Turetsky 2006, Kasischke et al., 2010) and temperature (Collins et al., 2013) in the Arctic and Subarctic, SOC could be significantly impacted in the CRB despite recovery of surficial organic materials following fire disturbance.

CHAPTER 2 –COST CONSTRAINED CONDITIONED LATIN HYPERCUBE SAMPLING STRATEGIES FOR REMOTE AREA ACCESS

SYNOPSIS

This work examined the utility of implementing a Conditioned Latin Hypercube Sampling (cLHS) methodology in order to locate optimal sampling locations in large, previously unmapped areas of remote Alaska. The cLHS used in this study was constrained by an inclusive cost layer representing an aggregation of real-world costs associated with travel within the Yukon-Kuskokwim Delta study area located in south western Alaska. To accurately represent costs associates with travel throughout the study area, a single inclusive cost layer was created by aggregating travel cost information from multiple modes of transportation including travel by helicopter, float plane, river boat, and commercial flight to villages located within the survey area. Performance of the cost-constrained cLHS method was analyzed by assessing the model's ability, constrained and unconstrained, to identify sampling locations that adequately represent a suite of environmental covariates and their feature space. Detailed analysis of cLHS model results for suggested sampling areas, with and without cost constraints, will aid in the creation of realistic sampling strategies that consider real-world scenarios and the optimal allocation of resources.

INTRODUCTION

The purpose of environmental sampling is to obtain data that enable predictions about a specific statistic, or group of statistics, over a larger area. The design of statistically sound environmental sampling procedures is especially important and useful in soil survey where soil properties are less obviously visible with satellite imagery or surface analysis. The survey of soils, and other materials at the earth's surface, can be optimized by making the best use of other data sources (i.e. covariates) in order to strategically select optimal sampling locations. Unlike soil survey efforts of the past that relied heavily on subjective decisions with few, if any, sampling sites being identified by quantitative procedures (Soil Survey Division Staff, 1993, Hewitt et al., 2008), soil scientists now have access to a large variety of detailed, digital datasets that when used in an effective manner have the ability to aid in the creation of sampling structure and design (Mulder et al., 2012; Roudeir et al. 2012; Scarpone et al., 2016; Sun et al., 2017).

Statistical sampling methods such as random (Howell et al., 2008) and stratified random (McKenzie & Ryan, 1999) sampling schemes have been previously used in the field of soil science to design sampling distributions that adequately capture spatial variability in the environmental covariates of a study area. While these methods may adequately sample geographic space, samples chosen by these methods may not cover the entire distribution of environmentally relevant covariates (feature space) which is particularly

important when attempting to design sampling strategies on large and diverse landscapes. Additionally, these sampling strategies may select areas for sampling that are impractical, or impossible, to travel to under realistic budgets and time constraints.

To address these shortcomings, Minasny and McBratney (2006) proposed Conditioned Latin Hypercube Sampling (cLHS) as a method for efficiently sampling the feature space of environmentally relevant covariates. cLHS is based on the concept of Latin Hypercube Sampling (LHS) (Iman, 1981), where a set of samples is taken from the feature space of an environmental covariate such that each sample set is maximally stratified. cLHS is a conditioned version of LHS that requires that the combination of samples drawn actually exist on the landscape. In addition to the conditioning of LHS to choose points that exist in the real world, the utilization of a cost layer, in the form a raster file, can further constrain cLHS model suggestions. Constricting cLHS by cost, allows the model to perform analysis while incorporating the cost of getting to sampling locations into the annealing schedule of the cLHS algorithm (Roudier et al., 2012; and Mulder et al., 2012). The further constriction of a cLHS model by cost is especially useful when attempting to perform soil surveys in large areas where the costs associated with travel can dictate accessibility across large areas and project feasibility.

Most notably, soil survey efforts in Alaska aim to map large, previously unsampled areas, containing very limited, or completely non-existent road networks. (Soil Survey Staff,

1995, 2005). Alaskan landscapes make up over 70% of remaining "not complete" (NOTCOM) soil survey acreage in the U.S. according to the United States Department of Agriculture - Natural Resource Conservations Services (USDA-NRCS) (Soil Survey Staff, 2019). Therefore, when conducting soil surveys in Alaska it is imperative to design sampling strategies that acknowledge real-world costs and barriers associated with travel in these remote areas. Previous studies have aimed to investigate cost-constrained cLHS performance by arbitrarily assigning cost values using other landscape variables such as surface roughness, land cover class, or distance from established road networks (Roudier et al., 2012, Mulder et al., 2012). While these estimations likely account for a significant source of relative variations in cost, cost values derived from the aggregation of real-world monetary cost data associated with multiple modes of travel would likely provide for more feasible sampling locations suggested by cLHS models.

The work outlined here examines the utility of implementing a cLHS method constrained by a multi-modal cost layer representing an aggregation of real-world costs associated with travel within the Yukon-Kuskokwim Delta study area located in south western Alaska. To accurately represent costs associates with travel throughout the study area, a single multi-modal cost layer was created by aggregating travel cost information from multiple modes of transportation including travel by helicopter, float plane, river boat, and commercial flight to villages located within the survey area. Performance of the cost-

constrained cLHS method was analyzed by assessing the model's ability, constrained and unconstrained, to identify sampling locations that adequately represent a suite of environmental covariates and their feature space. Detailed analysis of cLHS model results for suggested sampling areas, with and without cost constraints, will aid in the creation of realistic sampling strategies that consider real-world scenarios and the optimal allocation of resources.

MATERIALS AND METHODS

Study Area

Located in south western Alaska, the Yukon-Kuskokwim Delta (Y-K Delta) is bound on its northern border by the Yukon river and its southern border by the Kuskokwim river. This shared delta is the result of these two large rivers discharging water and sediment into the Bering sea. The Y-K Delta is the largest deltaic area in Alaska, occupying 1.3 x l05 km2 and is rivaled in size by the Mississippi delta which varies in size from 3.2 x l04 km2 and 1.2 x 105 km2 (Thorsteinson et al., 1989). The majority of soil surveys performed in this area of the state were concentrated to the east of the delta in the Yukon-Kuskokwim highlands (Soil Survey Staff, 1995, 2005) while little data are available for flat landscapes of the Y-K Delta to the west (Hinton et al., 1966; Knudson et al., 2004).

The Y-K Delta is located in the zone of discontinuous permafrost, and characterized by thaw lakes, meandering stream, organic rich peatlands, non-permafrost alluvial soils, and

coastal ecosystems. Elevations for the entire project area range from 0 m asl to 145 m asl. Soil parent materials in the Y-K Delta are dominated by a foundation of older alluvium, deposited from the Yukon and Kuskokwim Rivers, covered in many areas by a thin wind-blown loess or eolian sand cap (Soil Survey Staff, 2005). The specific study area boundary used in this work was created using an existing USDA-NRCS Major Land Resource Area (MLRA) boundary that includes the Y-K Delta in its entirety (Figure 8).

Road networks in the Y-K Delta are extremely limited (located only within villages), making travel in this area exceedingly difficult. Costs associated with travel in the Y-K Delta were modelled using Bethel and St. Mary's Alaska as possible travel origination points. Bethel, Alaska (population, 6,080 (US Census, 2010)) is the largest community in all of south western Alaska and is the most appropriate access point to the Kuskokwim river. In addition to being located on the Kuskokwim river, major floatplane and helicopter vendors serve Bethel and the surrounding area creating a centralized transportation hub in the Y-K Delta study area. St. Mary's, AK is the largest village on the Yukon River in the Y-K Delta and is located on the northeastern border of the study area, providing direct access to the Yukon river.

Latin Hypercube Sampling (LHS) Methodology

Latin Hypercube Sampling (LHS) is a statistical method for generating near-random stratified samples, or sample sets, from a multivariate distribution (McKay et al., 1979, Iman et al., 1981). In this study, multivariate distributions represent a suite of environmental covariates relevant to soil formation and in-situ processes. The LHS sampling method is an efficient way to model an empirical distribution function when attempting to represent large distributions containing many data points with much smaller distributions while preserving data coverage (Iman et al., 1981). This is accomplished by partitioning an original distribution, X, containing many data points, N, into a set of equal sized, non-overlapping strata and then randomly selecting one value within each stratum creating a hypercube. The end result of LHS is a set of data points, n, with distribution coverage, x, similar to the original data set, X, such that $n << N$. Benefits of LHS sampling are that there is no need to increase sampling points (strata) when adding variable distributions and that sample points within stratum are taken one at a time without replacement.

Conditioned Latin Hypercube Sampling (cLHS) Methodology

Although LHS sampling schemes have a high degree of utility and many advantages over random and random stratified sampling schemes (Minasny and McBratney, 2006), model outputs require *conditioning* to ensure that points generated by an LHS method actually

exist in the real world. The conditioned Latin Hypercube Sampling (cLHS) methodology attempts to solve this problem (Minasny and McBratney, 2006; Roudier et al., 2012; Mulder et al., 2012). Once the cLHS method selects a data set under the restriction that the data set needs to exist in the real-world, the data set is then tested using an objective function which provides assessment of how closely model chosen data sets resemble a perfect Latin Hypercube (i.e. does the perfect combination of variables required for a Latin Hypercube actually exist in one spot on the landscape). The objective function contained within this package is evaluated based on two major criteria:

1. Matching the sample with the empirical distribution functions of the continuous ancillary variables (environmental covariates)
2. Matching the sample with the correlation matrix of the continuous environmental covariates

When designing sampling strategies in areas that contain exhaustive coverage of environmental covariates, it is beneficial to attempt to cover as much of the range of values of each of the variables as possible. The challenge that cLHS attempts to solve is selecting sampling points which most effectively cover the entire range of distribution of

the feature space for all included variables (Roudier et al., 2011). This method can be thought of as an equal spatial coverage sampling strategy but rather than equally sampling geographic areas, the algorithm is attempting to equally sample feature space of some environmental variable relating to soil survey.

In addition to attempting to minimize an objective function, the model can also be further constrained by the associated cost involved with traveling to potential sampling locations. In this study we created a unique multi-modal cost raster that modeled real world costs of travel to locations within study area based off four diverse modes of transportation (helicopter, float plane, river boat, and on-foot) and their specific associated costs. When cLHS is constrained by cost the model attempts to minimize the objective and cost functions simultaneously. Effectively, the model is performing three main tasks: Attempting to maximize feature space coverage of multiple variable by selecting random points from pre-determined distribution strata (sample size), attempting to minimize an objective function as it relates to the real world existence of the combinations of variable values at any one location, and attempting to perform the previous two operations while limiting cost associated with each specific point. Objective function evolutions and minimizations are performed using a simulated annealing process contained within the cLHS model (Metropolis et al., 1953). This simulated annealing procedure mimics the controlled cooling process used to reach a global optimum for a targeted function.

Additionally, at each iteration of the annealing, costs are assessed via a cost layer and the cost of reaching any given point on the landscape is acknowledged.

Our Approach

For a typical soil survey, field campaign costs can be modeled using a simple function to describe the increase in cost as a person needs to travel away from a road network or from a specific starting point. Performing soil sampling procedures in an area as large and remote as the Y-K Delta with many different modes of transportation, all with specific cost functions associated with them, makes this problem more difficult to solve. In this work we explored the possibility of creating a single cost raster (layer) for the Y-K Delta study area that is an aggregate of multiple cost layers each describing costs associated with a single mode of transportation available in the region. This multi-modal cost raster was then used to constrain a cLHS model in order to determine sampling areas that not only covered feature space of environmental covariates but also considered costs associated with travel to individual locations. Here, we compared results between a cLHS method that was not constrained with our inclusive, multi-modal, cost raster (standard cLHS) and a model that was constrained by cost (cost-constrained cLHS). In addition to comparing points suggested by standard and cost-constrained cLHS we also compared results from models that included environmental covariate data for the entire land area inside the study boundary and results from models with covariate data removed for areas

that were inaccessible. The land areas deemed inaccessible included areas that were off-limits to sampling due to private or tribal land ownership where no pre-existing relationship existed. The inclusion of a model containing data for the entire land area within the Y-K Delta study boundary was motivated by the future possibility of gaining access to areas that are currently off-limits to sample. All cLHS models described in this study have been implemented using the R programming language (version 3.6.1, R Core Team, 2019) in the *clhs* package (Roudier 2011).

Environmental Covariates

The Y-K Delta study area has extensive coverage of spatial information from remotely sensed images, vegetation maps, and digital elevation models. Gooveaerts (1997) referred to this as exhaustive ancillary data where data is available at all locations. This exhaustive data (referred to here as "environmental covariates") is often useful for making spatial predictions, especially when primary information in a specific area is nonexistent. In order to better decide where to sample soils in the Y-K Delta study area a suite of six continuous environmental raster covariates (Figure 15) were used as input data for a cLHS model to propose specific sampling sites. Environmental covariate data that was used in our models was assumed to have some relationship to the formation and processes of soil formation. Landscape factors that influence soil formation include

climate, organism relationships, topography, base geologic material, and time. Environmental covariates included:

Digital elevation model (DEM) and derivatives

A digital elevation model obtained from (Gesch et al., 2002) sourced at 45 m pixel resolution. The DEM derivatives slope and normalized aspect were also used and processed in using the GDAL application within QGIS (QGIS Development Team, 2020). Here slope is a calculation of elevation differences between neighboring pixels. Normalized aspect was used as to quantify which cardinal direction each pixel on the ground faces. Normalization was performed by splitting pixels containing aspect data into "northing" and "easting". This is necessary as pixel values for aspect are circular meaning that the difference between values 360 and 1 would, without correction, be 359 degrees, where in reality these values are only 1 degree apart.

Normalized difference vegetative index (NDVI)

NDVI values were derived from spectral information from a late-season Landsat 7 Enhanced Thematic Mapper Plus mosaic (2008-2011) for each pixel. NDVI is a widely used calculation relating to "greenness" of pixels which help distinguish between vegetation classes. NDVI values were calculated as

$$(NIR - r)/(NIR + r) \qquad (1),$$

where NIR is near infrared light and r is red wavelength light.

Near Surface permafrost probability

Near-surface (<1 m) permafrost probability in Alaska (Pastick et al., 2015). This raster layer contains a random forest model prediction of the probability of the presence of permafrost within a 1 m of the surface. Model predictions for near-surface permafrost probability were produced using a suite of raster covariates described in Pastick et al., 2015.

Covariates not used

Certain environmental covariates were not included in this analysis such as land use/land cover, and DEM derived topographic wetness index. Model runtimes and computer power required significantly increase with the introduction of additional variables. In this

project we assumed NDVI could likely more sensitively account for major differences in land cover and land use than a derived, categorical product. Though topographic wetness index spatial data would include valuable information about soil processes and formations we found that elevation is not a major driver of soil function in this area and is adequately accounted for by a number of other covariates included within the cLHS model (DEM, normalized aspect, slope). Elevation throughout the area is relatively static and further derivation of the DEM allows for the potential to introduce noise or overfit model predictions.

Operational Cost Constraints

In addition to using a stack of environmental covariates, our particular cLHS model also used a multi-modal cost raster. This specific cost raster was created by aggregating multiple transportation methods by modeling their associated costs spatially. Specifically, cost layers were created to model costs spatially for travel by helicopter float plane, riverboat, and on-foot (Table 3). For float plane and river boat cost calculations, cost values were buffered two miles from the edges of float plane accessible water bodies and two miles from river center channels to represent a realistic distance a soil scientist carrying equipment could potentially travel on foot after traveling by main mode of

transportation. All cost rasters were created in QGIS version 3.14 using built in raster calculator functionality (QGIS Development Team, 2020).

Modes of Transportation

Helicopter

Costs associated with traveling in a helicopter were created by speaking to a local helicopter pilot in the area (Stan Hermann, personal communication) and utilizing price estimates of flight distances vs. cost (Table 3). Here, we used Bethel, AK and St. Mary's, AK as potential base points from which a helicopter could take off from, then created a function to describe the operating costs of traveling by helicopter to potential sample points. The minimum daily cost of travelling by helicopter ($4,000) accounted for all cost values within a 150 mile radius around helicopter take-off locations and covered most of the range of our study area (>95%) while costs outside of this boundary were calculated spatially to account for flights outside this minimum cost boundary (Figure 9). Costs outside of the daily minimum cost boundary were modelled to include the additional costs of having to make multiple trips in order to store fuel along travel routes to extend base helicopter ranges. Costs for travel by helicopter were calculated for each location contained in the study area as

$$Helicopter\ Travel\ Cost = \frac{T_h * (D_h - D_{\min})}{V_h} * C_{he} \quad (2),$$

where Th is a travel constant related to the amount of total trips required for departure and return flights, Dh is the total distance travelled in miles, $Dmin$ is the range covered by the minimum daily cost in miles, Vh is the velocity of the helicopter in miles per hour, and Che is the cost associated with an extension outside of the boundary created by the minimum daily cost in dollars per hour.

Float plane

Costs associated with travel by float plane were spatially modelled by using Bethel, Alaska as a starting point from which a floatplane can take off from. In this scenario our aircraft is only able to land on bodies of water as it is not equipped with other types of landing gear. Additionally, water bodies must meet minimum surface area criteria to ensure safe take-off and landing procedures. Minimum water body area sizes were set at 3 km^2 with the assistance of a local pilot that frequently operates within this area (Aaron Ostanoski, PapaBear Adventures, personal communication). Once only adequate bodies of water were selected, a two-mile buffer was created around each body of water (Figure 10). This two-mile buffer was selected as a feasible distance a team could travel on foot from an established base camp with soil sampling equipment to perform soil sampling

procedures. Once adequate waterbodies were selected and buffered, costs for travel by float plane were calculated for each 45 m pixel contained in the study area as

$$Float\ Plane\ Travel\ Cost = \frac{T_f * D_f}{V_f} * C_f \quad (3),$$

where *Tf* is a travel constant related to total trips required for departing and return flights, *Df* is the total distance travelled by the float plane, *Vf* is the velocity of the float plane in miles per hour, and *Cf* is the operational cost of the float plane in dollars per hour.

River boat

Travel by river boat was spatially modelled using Bethel, AK and St. Mary's, AK as potential base points from which a boat could launch from starting on the Kuskokwim and Yukon rivers respectively (Figure 11). In addition to modeling costs originating from Bethel, AK up and down the Kuskokwim river, cost was also modelled for a short section of the Gweek river (a tributary of the Kuskokwim). Guidance on which routes were acceptable for travel was provided by a local riverboat operator with local knowledge of navigable waters (Fran Reich, personal communication). Cost was modelled using a function that included river distances, boat speed, and boat hourly costs. These spatial

models extended 30 river miles up and down stream and were buffered 2 miles from the center of the river channel in an effort to keep points within a realistic travel distance for a day long sampling trip by foot to and from a boat landing location. Costs were calculated for location in the study area as

$$River\ Boat\ Travel\ Cost = \frac{D_b}{V_b} * C_b \quad (4),$$

where D_b is the total distance travelled by the river boat, V_b is the estimated velocity of the river boat, and C_b is the operational cost of the riverboat in dollars per hour.

Sampling on foot from village centers

In addition to more elaborate methods of travel, we also modeled the cost of flying commercially to remote villages contained within the Y-K Delta study area with flights departing from Bethel, Alaska (Ravn Air Alaska, 2020). Flight costs were modelled by gathering airfare cost data for each village and then buffered this cost to a 2-mile radius outside each village center (Figure 12). While the total area that is possible to sample with this travel method is relatively small compared to the Y-K Delta study area, costs associated with commercial airfare and on-foot sampling are relatively low compared to other methods of travel.

Inclusive Multi-Modal Cost Raster.

Costs for each method were modelled individually and then combined into one inclusive, multi-modal cost layer. During aggregation of individual cost layers, a lowest value function was used to assign the lowest possible travel cost for single areas that could be reached by multiple modes of transport (Figure 13). When creating individual cost rasters, each cell value was rounded to the nearest dollar amount and was given a decimal place identifier to later aid in investigating which specific travel method costs were calculated from for locations where multiple methods overlap. This inclusive, multi-modal cost raster allows for the ability to design sampling schema based on quantitative analysis of remotely sensed variability within an area coupled with the cost associated to physically travel to these locations.

RESULTS & DISCUSSION

Model Selected Sampling Locations

Figure 14 shows sample locations over 100 realizations for both the standard and cost-constrained cLHS methods are mapped for Nunivak Island (located on the western boundary of Y-K Delta study area) and illustrates the differences in spatial structure of the locations selected by cost- constrained and standard cLHS models. Point densities clearly illustrate how the cost-constrained cLHS model considers cost when attempting to select sampling locations by preferentially selecting areas that are located in lower cost regions.

In addition to analyzing individual points within the study area based on spatial structure, a gaussian kernel density function (estimated using a search radius of 5000 m) was applied to the sample locations to illustrate the spatial distribution of proposed sampling locations (Figure 15). This was done by merging sample area recommendations over 100 realizations and calculating how many points were within a predetermined search radius. The proposed sample locations suggested by the cost-constrained cLHS method appear to be clustered in specific areas when compared to the proposed sampling locations suggested by the standard cLHS method which seem to be more evenly distributed across the landscape. Points are likely to be closer to bodies of water or within a nearer to travel origination locations, making them easier to reach and more cost effective for soil

scientists performing field sampling. This is clearly illustrated by the point density increase near Bethel, AK, when comparing cost-constrained to standard cLHS methods. With the removal of cost constraints, the standard cLHS selecting a point located near an easily accessible lake and a point thousands of miles away in a remote basin would be equiprobable. This is visually apparent by the lack of density in the standard cLHS model suggested points compared to the cost-constrained cLHS suggested points.

Kernel Density Map Search Radius

General sampling areas rather than precise point locations where selected by aggregating model suggested points over 100 realizations and then analyzing point densities within a certain search radius. Due to the large size of the Y-K Delta it is unlikely that two points would fall in close proximity even after 100 realizations of the model. Here, search radius was slowly increased and histograms of point density vs. frequency could be used to select a search radius that is large enough to display point density results in a meaningful way (Figure 16). While areas that show as high density (red) on the map are large and not likely useful in selecting a specific point on the ground to sample, these maps can still be useful in determining general vicinities that cLHS models selected multiple times. Investigations of adequate search radius for kernel density maps were calculated using data extracted from models using only data located in areas where access is permitted.

Environmental Covariate Distributions

Original distributions of environmental covariate data were compared to model selected distributions over 100 realizations of each cLHS method (cost-constrained and standard) (Figure 17). Model results for slope and elevation appear to be slightly under sampled by the cost-constrained cLHS method. This is most likely due the areas with large changes in elevation and slope being further distances away from origination points for travel (Bethel and St. Mary's, AK) and therefore being heavily penalized by the cost layer. While there is some under sampling being performed by the cost-constrained cLHS model it can be seen that there is adequate feature space coverage for each covariate by both the cost-constrained and standard cLHS method. All else being equal it appears it is a more efficient use of resources to sample areas suggested by the cost-constrained model as they offer similar coverage while taking into account the costs associated with traveling to specific areas. Covariate distribution comparisons were calculated using data extracted from models using only data located in areas where access is permitted. Distribution coverage for models utilizing all land data showed similar results and trends (Figure 23).

Model Presets

When performing sample site selection using a cLHS method, model runtimes and computational burdens can be optimized by selecting reasonable model presets. The purpose of this project was not only to design a sampling site selection procedure that could maximize the capture of variability while minimizing cost, but also to design a sampling protocol that could be implemented in the real world.

The cLHS model that was used in this study has a user defined number of iterations it will perform while trying to minimize an objective. The objective function can be thought of as a representation of how close data points chosen by the model relate to a theoretical Latin Hypercube. In order to better optimize model runtime and the minimization of the objective function, 10 realizations of the cLHS model were performed, with the model set to run 20,000 internal iterations. From these realizations it is possible to locate a point of diminishing return (inflection point) where the model is no longer rapidly minimizing the objective function (Figure 18). For the purposes of this particular study 5,000 internal iterations were chosen for all model runs as the objective function was minimized in a meaningful way and model run times were appropriate for real world time and computational constraints.

Additionally, the cLHS models presented in this study were set to operate on a limited number of points on the landscape from which they could extract environmental covariate

data from. This was performed by gridding the study area with a pre-determined number of vertices and extracting data only at these points for the models to use. Ideally, we would use every single pixel contained within the study area as its own data point and allow the model to select values from the entire distribution. However, for an area as large as the Y-K Delta using every pixel would result in a data frame of ~40 million observations and model runtimes would drastically increase (Figure 19). When analyzing feasible model runtimes, we decided that ~10 million vertices would be a realistic number to use. 10 million equally gridded vertices within the Y-K Delta study area translate to on the ground areas of 0.03 km^2, which are reasonably sized areas to conduct soil inventory.

Cost Differences Between cLHS Methods

When cost constraints are included in modelling, internal cLHS model iterations attempt to minimize the cost while simultaneously minimizing the objective function (Figure 20). While both methods appear to be minimizing the objective function, which relates to how close the sample is to an actual Latin hypercube, the standard cLHS model appears to be more effective. This is because there are no constraints being applied to the standard method and the data chosen by the model is attempting to only accomplish one task. The difference between the evolution of the objective function for each method illustrates the

trade-off that needs to be considered when applying cost constraints to a cLHS model. Decisions about constraining a cLHS model by cost can be further explored by comparing total costs to travel to selected point selected by each model (with and without cost constraints).

Selected sample points for standard cLHS and cost-constrained methods were aggregated over 100 realizations and then independently analyzed by extracting cost values of each point from the cost raster for the study area. This allows for the comparison of real-world costs associated with travelling to sampling points suggested by these different models. Average total cost was significantly higher ($p < 0.001$, Welch's two sample t-test) when calculated using sample points selected by standard cLHS models, averaging $383,786 ± 2,285 US dollars, compared to an average cost of $298,245 ± 12,287 USD dollars when incorporating cost-constraints (Figure 21). This information is especially interesting for land managers when planning soil sampling strategies for field use. A careful analysis of cost to travel to specific areas, especially in areas that have multiple methods of travel, can result in similar environmental covariate data coverage for significantly lower overall costs.

Implications for future sample site selection using cLHS for remote areas in Alaska

While the Y-K Delta has exhaustive geospatial information related to soil formation and processes, cLHS requires environmental covariate input data to be consistent resolutions. Most covariate data in the Y-K Delta region that covers our study area entirely is available at a 45m pixel resolution which limits potential for highly accurate representations of specific areas on the ground. While it would be possible to gather higher resolution data for specific zones within the larger study area, doing so has the potential to introduce bias into the model as some areas would contain much higher resolution data than others.

In addition to limitations with input data, real world time and budget constraints largely affected decisions made when performing model calculations and designing this study. This specific soil sampling campaign was designed to be completed over a period of three to four years with field sampling campaigns averaging four weeks each year. Considering the size of the study area, difficulty of transportation logistics, and costs associated with travel it was estimated that 100 sampling locations was a realistic number that could potentially be visited with these limitations. Once high point density locations are designated by the model, a qualified soil scientist equipped with experience and knowledge of the landscape could use model designated areas to aid in the placement of precise sampling locations.

Lastly, the current cLHS models widely available in R (Roudier et al., 2011) calculate costs of traveling to each point location independently and does not acknowledge the possibility of visiting multiple points without returning to an origination point. Further work should focus on solving this problem by implementing travel network optimization into the current cLHS model. This would allow for the evaluation of the combined cost of visiting multiple points along an optimally chosen route and would more closely resemble real-world soil sampling strategies.

CONCLUSIONS

In this work a method to add operational cost constraints to the cLHS algorithm was proposed and tested using a data set in the remote Yukon-Kuskokwim Delta area of western Alaska. This method attempts to better quantify the costs associated with travel to and from potential soil sampling locations by modelling different modes of transportation available within the study area, aggregating them into a single cost layer to guide the cLHS algorithm toward choosing cost-effective sampling locations. During development of this cost raster, values were modelled specifically to approximate actual costs (in USD) to travel to these specific areas. Cost functions were created with the assistance of local airplane, helicopter, and riverboat operators and were based on current

prices of travel. In order to produce accurate predictions of costs into the future, cost values would likely need to be updated on some predetermined time interval.

In this study, a cost-constrained cLHS selected data sets that adequately represented original environmental covariate feature space and as such is an appropriate method for designing sampling strategies. While some programming skill is required, it is our hope that similar workflows can be implemented to aid in the determination of where to sample soils in order to capture maximum variability all the while minimizing costs associated with field-based sampling campaigns. There are many ways that cLHS model predictions can be improved with the addition of more environmental covariates or running models for longer on larger computers. However, this study aimed to explore cLHS operations was under realistic time and budget constraints and was designed in a way that produced sample collection procedures that can actually be implemented.

Tables and Figures

Table 1. Forestry metrics and soil characteristics for late successional and post fire black spruce plots in the Copper River Basin, Alaska.

	Post Fire (PF)	Late Successional (LS)
Tree Characteristics		
Live Stem Density (trees ha-1)	3,380 ± 1,621a*	3,047 ± 1,386a
Stand Age (years)	94 ± 14a	206 ± 29b
Height of Trees (m)	3.4 ± 1.3a	5.4 ± 2.1b
dbh of Trees (cm)	4.5 ± 1.0a	6.5 ± 1.8b
Seedling Density (stem ha-1)	6,238 ± 3,279a	7,050 ± 2,929a
Soil Characteristics		
Fibric† organic (Of) Thickness (cm)	12.2 ±3.3a	10.5 ± 4.3b
Mesic‡ organic (Om) Thickness(cm)	2.9 ± 4.2a	3.2 ± 4.8a
Humic§ organic (Oh) Thickness(cm)	10.5 ± 5.2a	16.7 ± 9.9b
Organic Layer Thickness (cm)	25.6 ± 7.4a	30.4 ± 10.5a
Depth to Permafrost (cm)	55.6 ± 11.9a	89.5 ± 27.0b

*Different letters between columns in the same row indicate significant ($p < 0.05$) differences between post fire (n = 22) and late successional (n = 22) plots using Welch's two sample T-Test.
†Fibric (Of) organic materials in the Canadian System of Soil Classification (Soil Classification Working Group, 1998) are equivalent to fibric (Oi) materials in U.S. Soil Taxonomy (Soil Survey Staff, 2014).
‡ Mesic (Om) organic materials in the Canadian System of Soil Classification (Soil Classification Working Group, 1998) are equivalent to hemic (Oe) materials in U.S. Soil Taxonomy (Soil Survey Staff, 2014).
§ Humic (Oh) organic materials in the Canadian System of Soil Classification (Soil Classification Working Group, 1998) are equivalent to sparic (Oa) materials in U.S. Soil Taxonomy (Soil Survey Staff, 2014).

Table 2. Mean and standard deviations of soil organic carbon (SOC) concentrations, soil organic carbon densities, soil pH, gravimetric water content (θ_g), and soil bulk density for standardized depth increments under late successional and post fire black spruce stands in the Copper River Basin, Alaska.

	0-20 cm		20-50 cm		50-100 cm	
	Post fire	Late Successional	Post fire	Late Successional	Post fire	Late Successional
SOC (g $100g^{-1}$)	32.2±5.4a	32.3±5.8a	8.4±5.3a	9.7±3.9a	2.7±.6a	2.7±0.6a
Carbon density (kg C m^{-2} cm^{-1})	0.31±0.10a	0.79±0.29b	0.24±0.12a	0.42±0.20b	0.10±0.03a	0.14±0.03b
pH	5.6±0.4a	4.9±0.5b	6.6±0.1a	6.0±0.2b	7.2±0.3a	6.7±0.2b
θ_g (g H_2O g $soil^{-1}$)	312.9±19.8a	214.1±7.7b	98.2±65.1a	93.9±36.9a	59.9±7.3a	68.8±11.3b
Bulk density (g cm^{-3})	0.2±0.1a	0.3±0.2b	0.9±0.2a	0.9±0.1a	1.0±0.05a	1.0±0.1a

*Different letters between columns in the same depth increment indicate significant ($p < 0.05$) differences between post fire ($n = 22$) and Late Successional ($n = 22$) plots using Welch's two sample T-Test

Table 3. Frequency of occurrence of common shrub, forb, graminoid and bryophyte species in late successional and post fire stands under *P. mariana* (black spruce) in the Copper River Basin, Alaska.

Species	Occurrence Frequency (%)		χ^{2*}	p
	Late Successional	Post fire		
Arctostaphylos rubra	97	95	1.14	0.28
Aulocomium spp.	52	91†	**9.88**	**< 0.01**
Betula glandulosa/nana	10	0	3.53	0.06
Carex spp. ‡	93	91	0.08	0.77
Empetrum nigrum	100	95	1.78	0.19
Equisetum palustre	79†	36	**9.90**	**< 0.01**
Equisetum scirpoides	72	68	0.11	0.74
Geocaulon lividum	10	9	0.02	0.88
Grasses§	97	100	1.14	0.28
Hylocomium splendens	87	91	0.28	0.60
Pedicularis labradorica	3	0	1.14	0.28
Petasites frigidum	69	45	2.86	0.09
Polygonum alpinum	83†	50	**6.28**	**0.01**
Potentilla fruticosa	79	63	1.53	0.22
Rhododendron groenlandicum	100	100	0	1
Rosa acicularis	3	41†	**12.02**	**< 0.01**
Rubus chamaemorus	90	82	0.64	0.42
Salix spp.	100	100	0	1
Senicio spp.	72	50	2.69	0.10
Vaccinium uliginosum	100	100	0	1
Vaccinium vitis-idea	100	100	0	1

*Chi-square statistics (χ^2) and related P-values are from ANOVA tests on binary presence- absence data for the effects of site category on species frequency.

†Indicates significantly greater frequency ($p < 0.05$) of occurrence in either late successional or post fire categories based on analysis of deviance (Type II) results on chi-square statistics.

‡*Carex* spp. are predominantly *C. lugens* and *C. aquatilis*

§Grasses include species of the genus *Calamagrostis* and *Arctagrostis*

Table 4. Yukon-Kuskokwim delta study area ravel cost equation parameter symbols, units, and values

Variable Name	Units	Symbol	Value
Helicopter			
Travel Constant	-	T_h	4
Distance Range for Minimum Cost	mi	D_{min}	150
Velocity	mi hr^{-1}	V_h	75
Cost of Extension	\$ hr^{-1}	C_{he}	1,000
Distance Travelled	mi	D_h	-
Float Plane			
Travel Constant	-	T_f	4
Velocity	mi hr^{-1}	V_f	150
Cost	\$ hr^{-1}	C_f	200
Distance Travelled	mi	D_f	-
River Boat			
Trip Constant	-	T_b	
Velocity	mi hr^{-1}	V_b	8
Cost	\$ hr^{-1}	C_b	100
Distance Travelled	mi	D_b	-

Parameter units, symbols, and values used in the calculation of cost associated with a specific method of transportation throughout the Yukon-Kuskokwim Delta study are

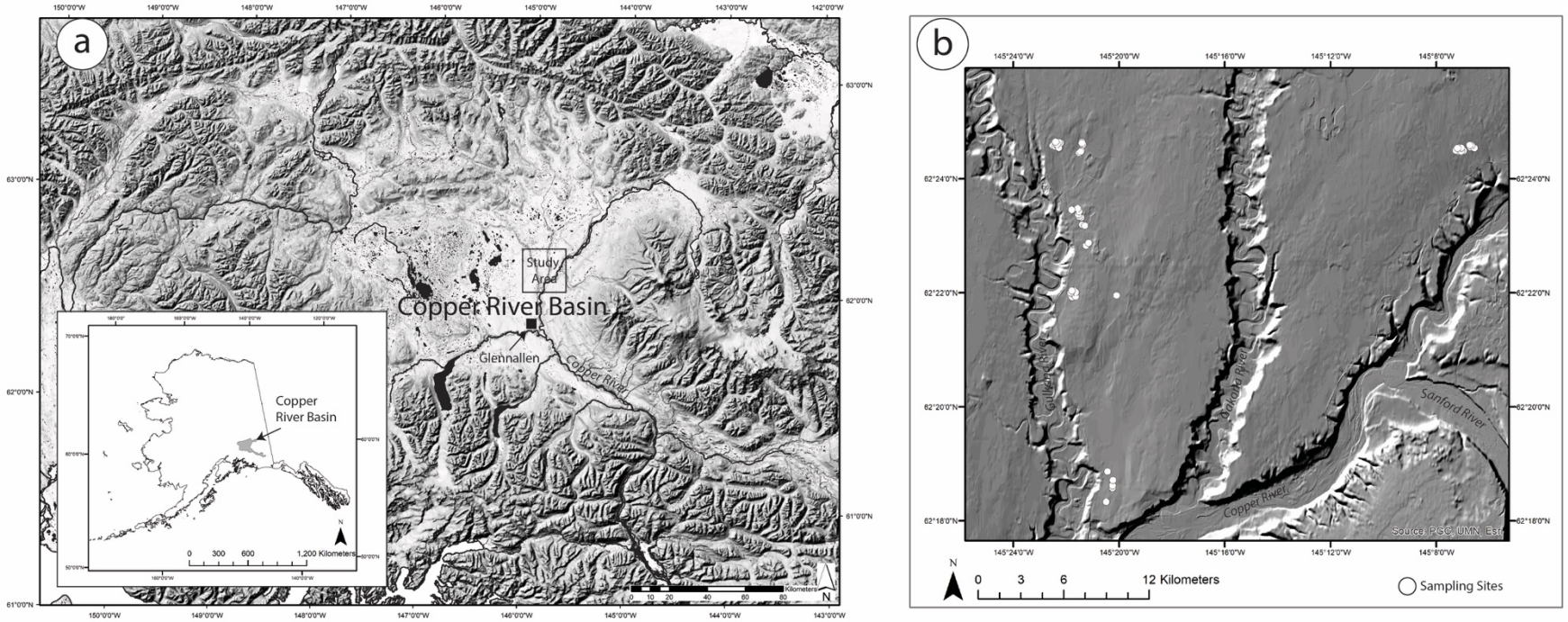

Figure 1. (a) Physiographic context of the Copper River Basin (CRB) (south-central Alaska, inset), located in the intermontane basin between the Alaska Range (north), Wrangell Mountains (east), Chugach Mountains (south), and Talkeetna Mountains (west). The extent of the CRB physiographic region largely follows the boundaries of the maximum extent of Glacial lake Ahtna, with the exception of the northwestern area intruding into the Talkeetna Mountains. (b) Hillshade (ArcticDEM) showing location of sampling plots (n = 44) on the glaciolacustrine plateau of the CRB, which has been incised by the Copper River and its tributaries. Figure creation performed in QGIS using Arctic DEM (Porter et al., 2018; QGIS Development Team, 2020)

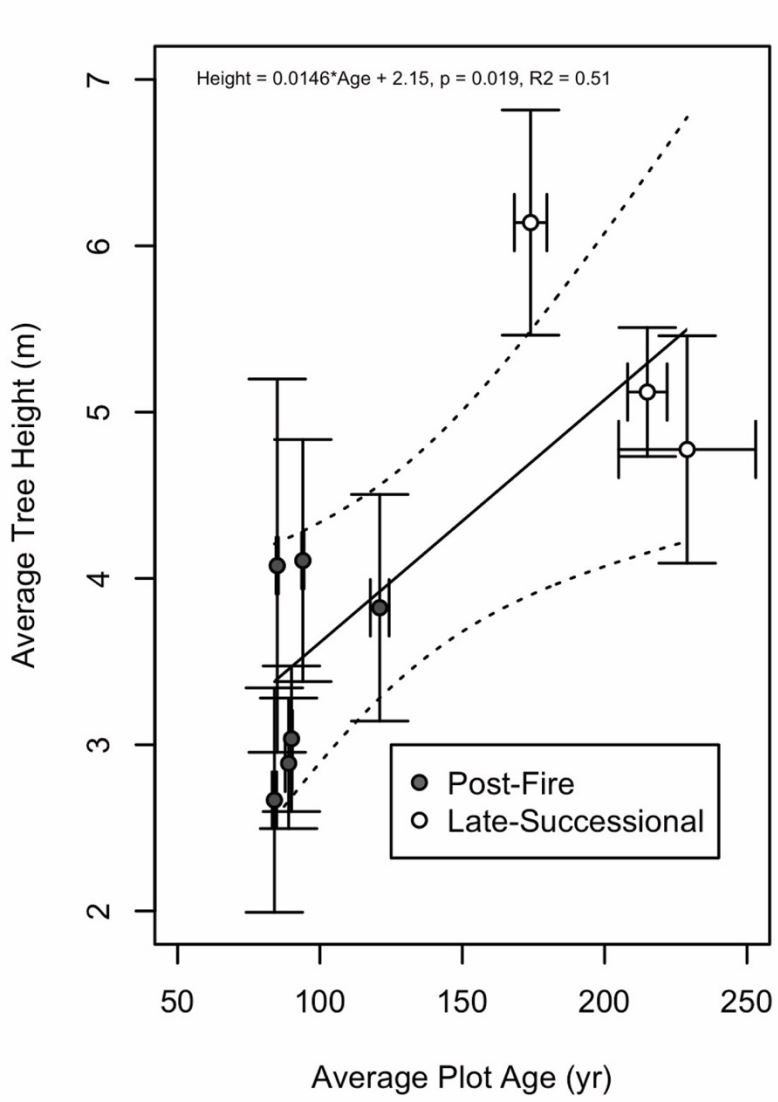

Figure 2. Relationship between average plot age (average plot age on the x-axis represents the average age of plots in each cluster as estimated by the protocol outlined in section 2.2) and tree height (m) for black spruce (P. mariana) trees in post fire (PF) plot clusters (grey) and late successional (LS) plot clusters (white) in the Copper River Basin, Alaska. The dotted line represents the 95% confidence interval around the slope of the linear regression line, and error bars represent standard errors for cluster averages of plot age and tree height.

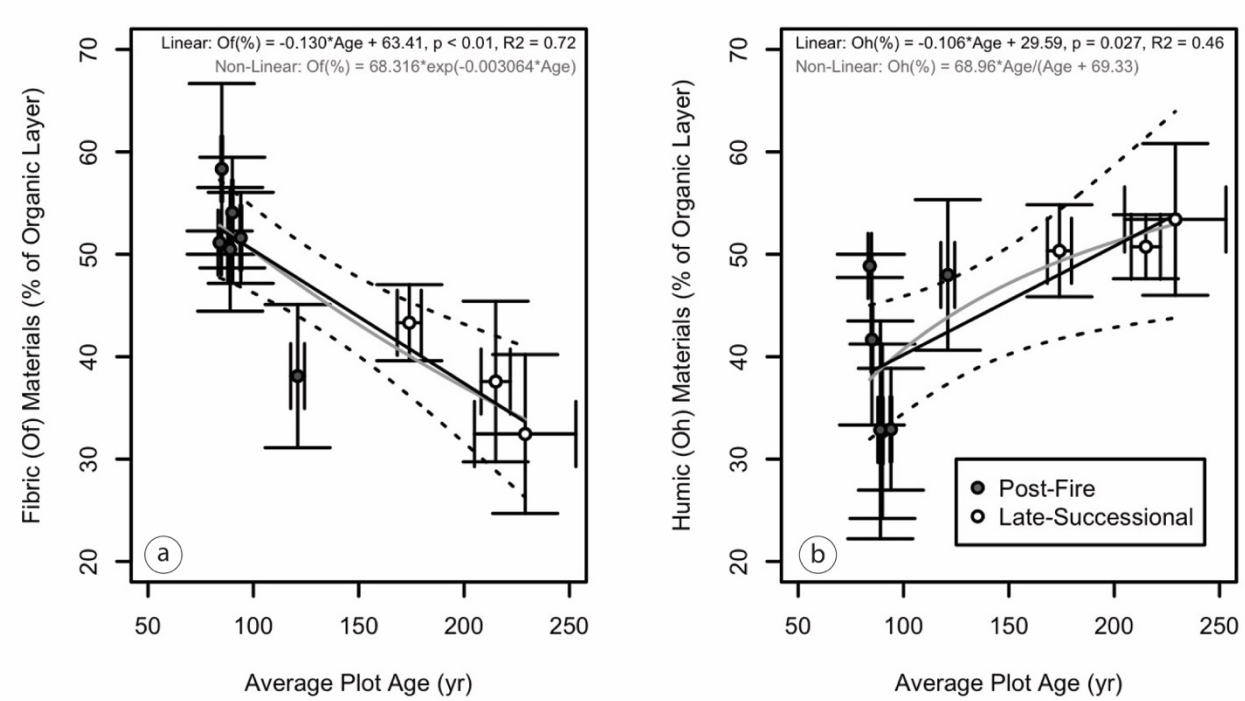

Figure 3. Relationship between average plot age (average plot age on the x-axis represents the average age of plots in each cluster as estimated by the protocol outlined in section 2.2) and a) the percent of the total organic layer thickness made up of fibric (Of) materials, and b) the percent of the total organic layer thickness made up of fibric (Of) materials for post fire (PF) plot clusters (grey) and late successional (LS) plot clusters (white) in the Copper River Basin, Alaska. The dotted line represents the 95% confidence interval around the slope of the linear regression line, and error bars represent standard errors for cluster averages of plot age and organic layer composition. Non-linear exponential decay (a) and Michaelis-Menten asymptotic increase (b) models (solid grey lines) were also fitted to the data (Archontoulis et al., 2015).

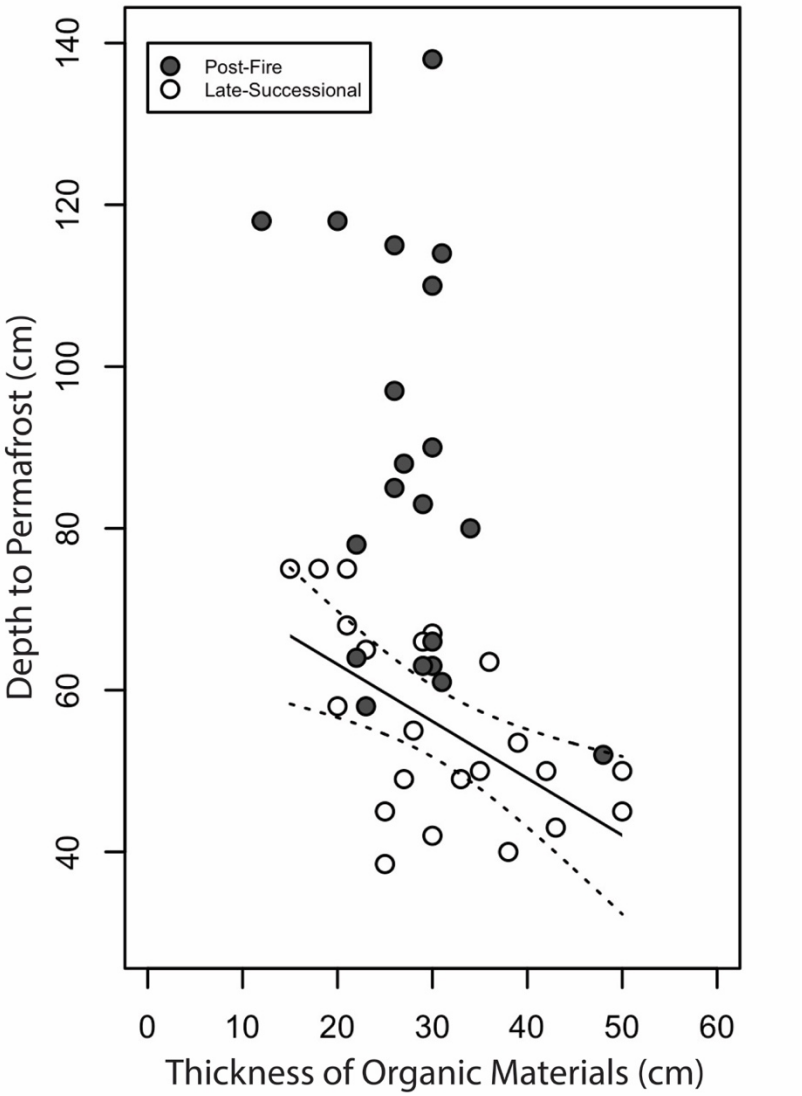

Figure 4. Relationship between organic layer thickness (OLT) and observed depth to permafrost across 44 investigated plots under post fire (grey, n = 22) and late successional (white, n =22) black spruce (P. mariana) in the Copper River Basin, AK. Depth to permafrost on late successional plots was linearly related to organic layer thickness (OLT): (Depth to permafrost (cm) = -0.7044*OLT + 77.28, R2 = 0.31, $p < 0.001$). The dotted line represents the 95% confidence interval around the slope of the regression line. For post fire plots, there was no significant linear relationship between depth to permafrost and OLT ($p > 0.13$).

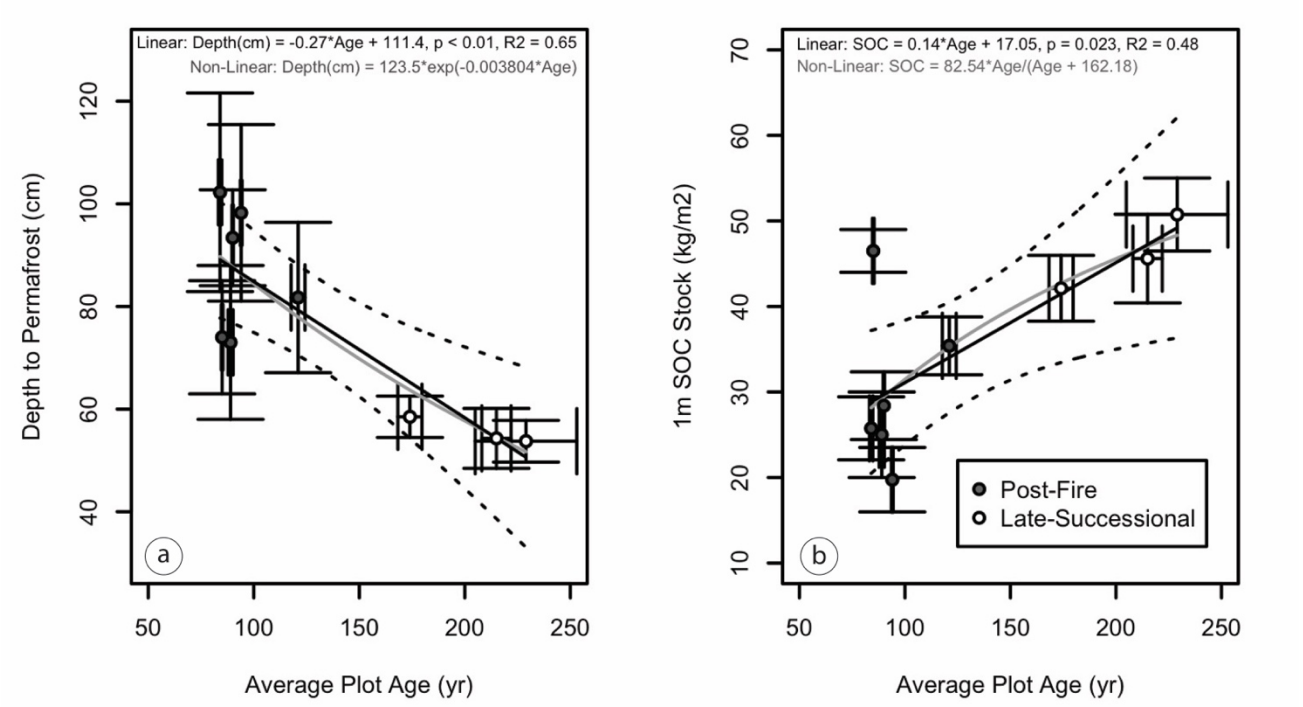

Figure 5. Relationship between average plot age (average plot age on the x-axis represents the average age of plots in each cluster as estimated by the protocol outlined in section 2.2) and a) depth to permafrost, and b) 1m soil organic carbon (SOC) stocks for post fire (PF) plot clusters (grey) and late successional (LS) plot clusters (white) in the Copper River Basin, Alaska. The dotted line represents the 95% confidence interval around the slope of the linear regression line, and error bars represent standard errors for cluster averages of plot age and organic layer composition. Non-linear exponential decay (a) and Michaelis-Menten asymptotic increase (b) models (solid grey lines) were also fitted to the data (Archontoulis et al., 2015).

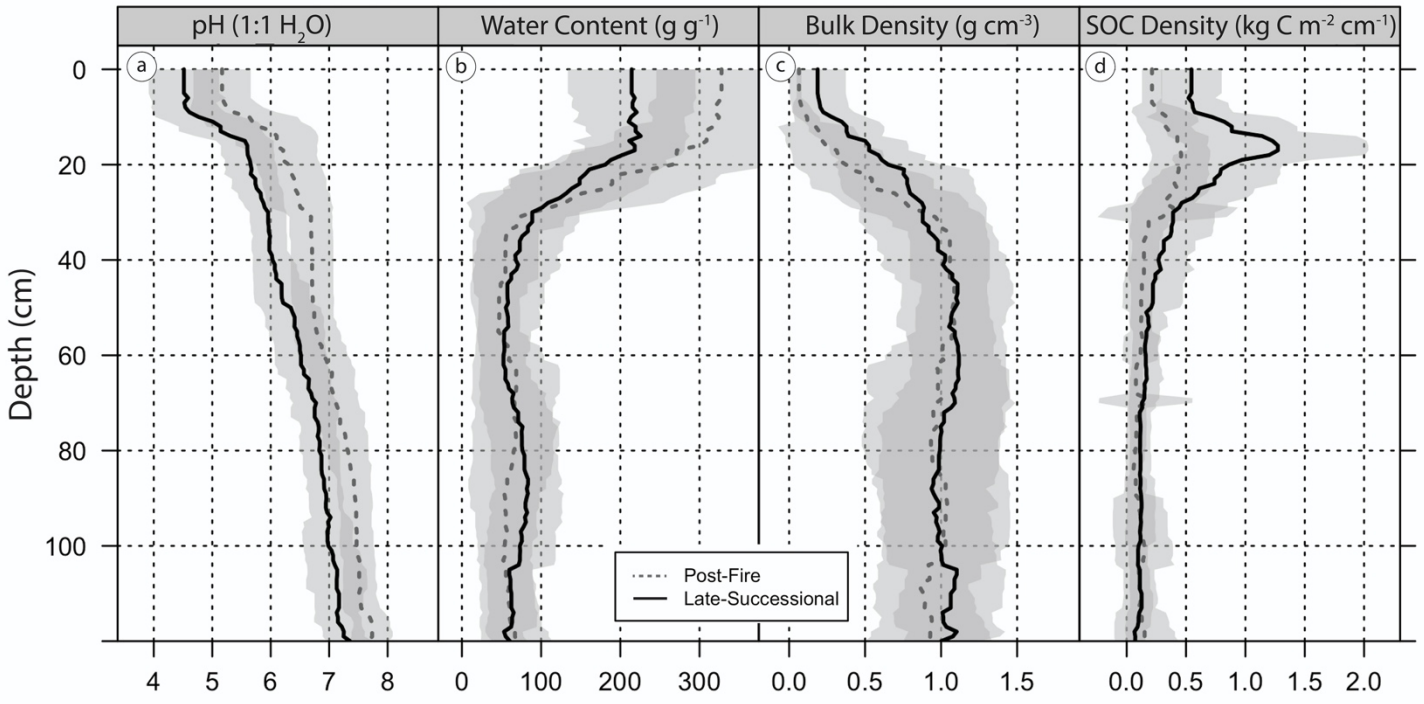

Figure 6. Depth trends of average (a) pH (1:1 H2O), (b) gravimetric water content (g H2O g soil-1), (c) bulk density (g soil cm3), and (d) soil organic carbon density (kg C m-2 cm depth-1) in soils across post fire (black, dashed) and late successional (black, solid) black spruce (P. mariana) plots in the Copper River Basin, AK. The solid and dashed lines represent the "slabbed" averaged for every 1-cm increment for post fire (n = 22) or late successional (n = 22) plots (using the Algorithms for Quantitative Pedology (AQP) package in R [Beaudette et al., 2013]). The gray zone represents plus or minus 1 standard deviation from the mean.

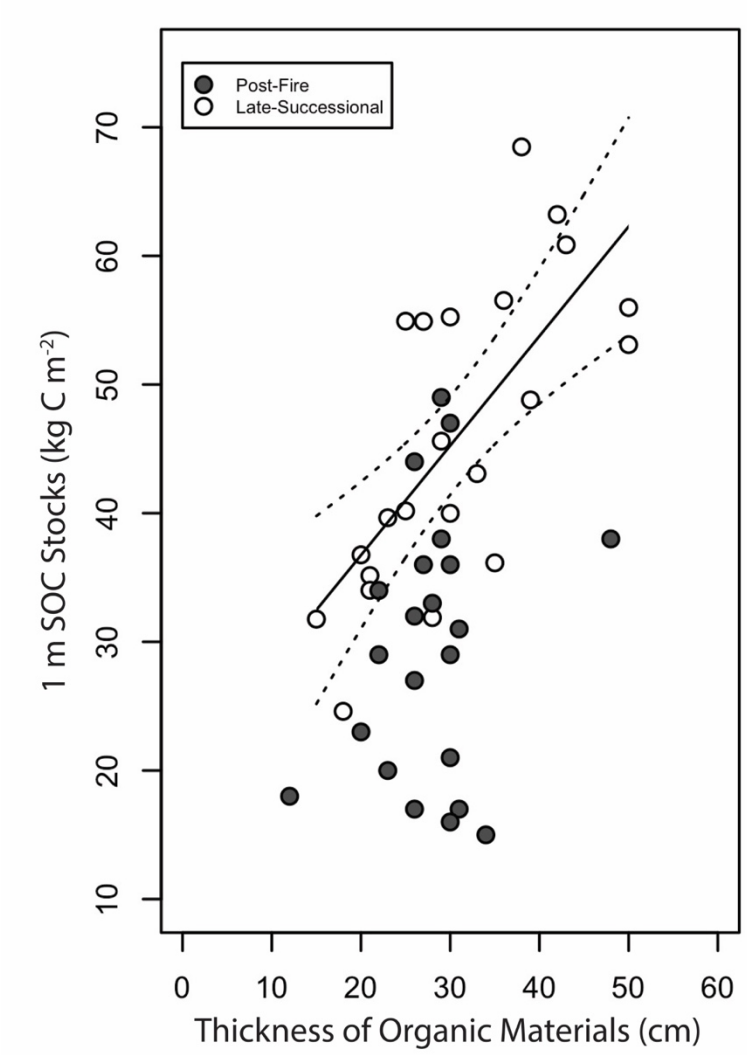

Figure 7. Relationship between organic layer thickness (OLT) and 1 m soil organic carbon (SOC) stocks across 44 investigated plots under post fire (grey, n = 22) and late successional (white, n =22) black spruce (P. mariana) in the Copper River Basin, AK. 1 m SOC stocks in late successional plots were linearly related to OLT (1 m SOC stock kg C m-2 = 0.8515*OLT + 19.71, R2 = 0.48, $p < 0.001$). The dotted line represents the 95% confidence interval around the slope of the regression line. For post fire plots, there was no significant linear relationship between 1 m SOC stocks and OLT ($p > 0.30$).

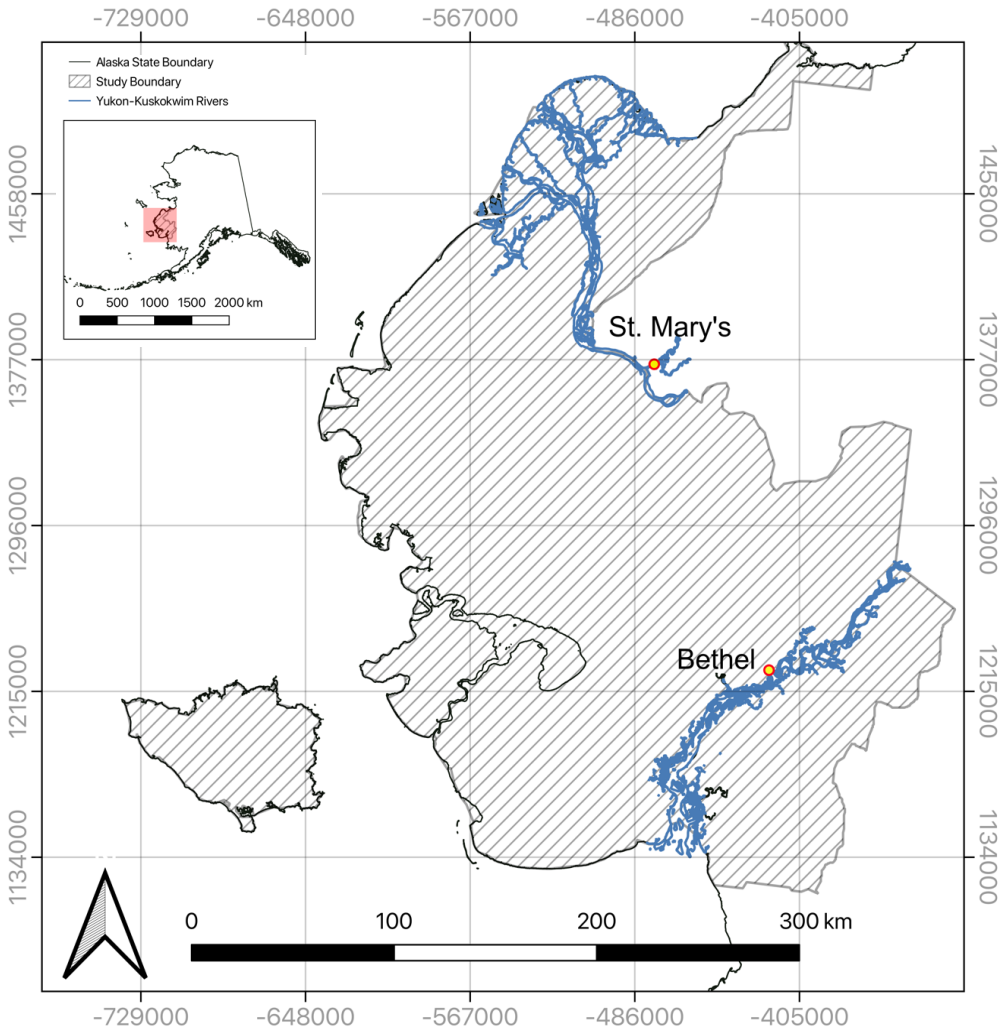

Figure 8. Geographic context of the Yukon-Kuskokwim Delta study area (Y-K Delta) (south western, Alaska, inset), located in the lowland delta between the Yukon River (north), and Kuskokwim River (south). The extent of the Y-K Delta study area largely follows the boundaries of these two major rivers in Wester Alaska. Figure creation was performed in QGIS version 3.14 (QGIS Development Team, 2020).

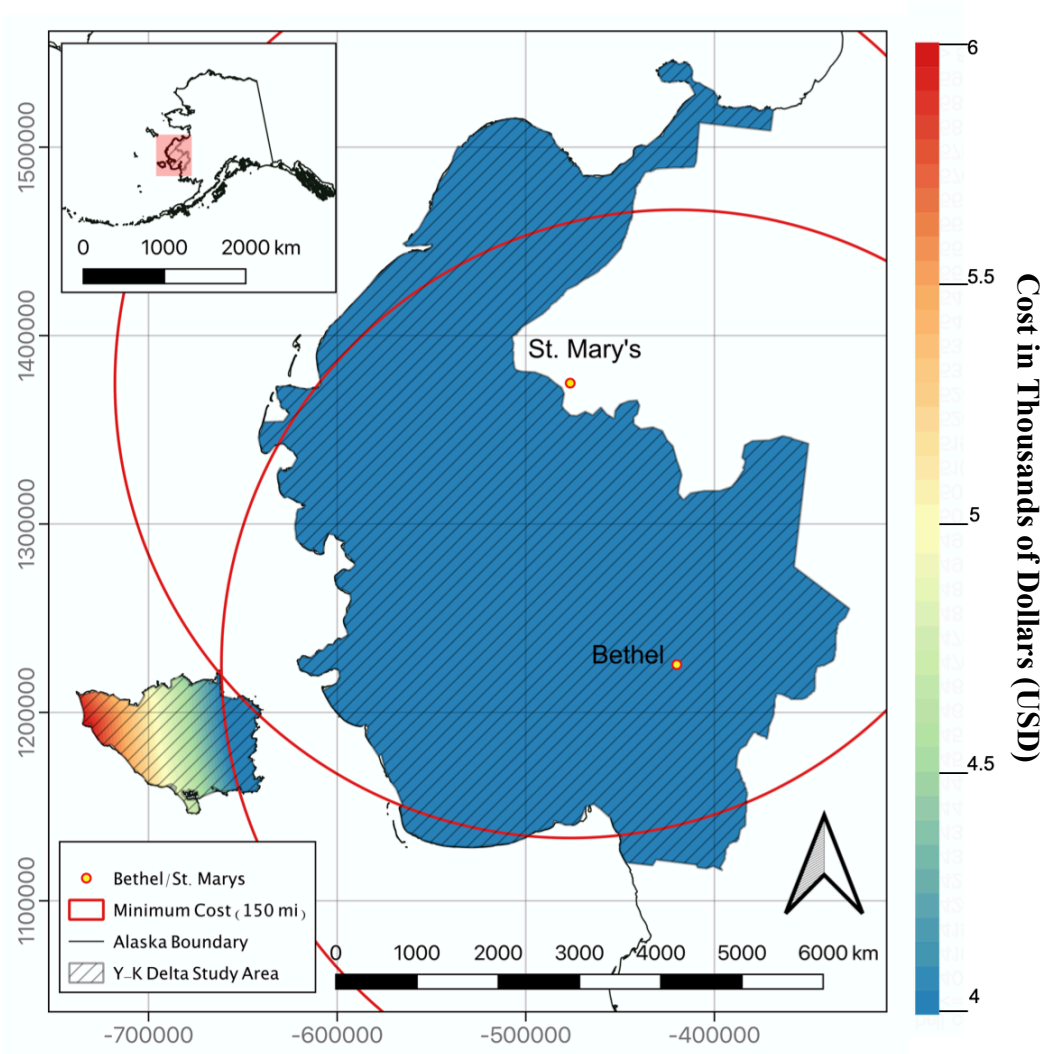

Figure 9. Costs associated with travel by helicopter modelled for the Yukon-Kuskokwim Delta study area (south western Alaska inset) in thousands of dollars (USD). Red circles show the area within the daily minimum operational cost of travelling in a helicopter taking off from the villages of Bethel and St. Mary's Alaska ($4,000). Figure creation performed in QGIS version 3.14 (QGIS Development Team, 2020).

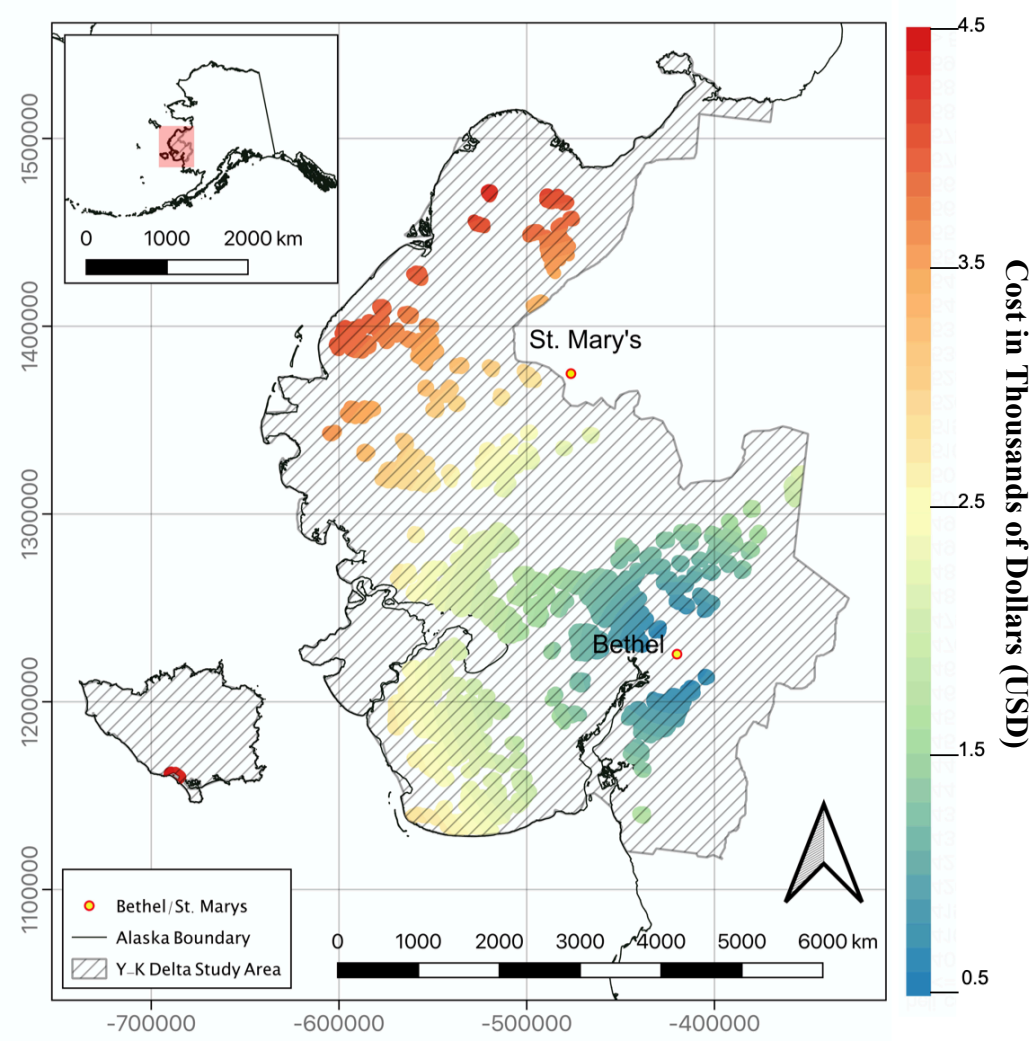

Figure 10. Costs associated with travel by float plane (in thousands of dollars (USD)) for the Yukon-Kuskokwim Delta (Y-K Delta) study area (south western Alaska, inset). Costs were calculated using a subset of waterbodies with an adequate surface area for safe take-off and land operations. Colored areas show how costs increase as distance from float plane take-off location (Bethel, Alaska) increase. Figure creation performed in QGIS version 3.14 (QGIS Development Team, 2020).

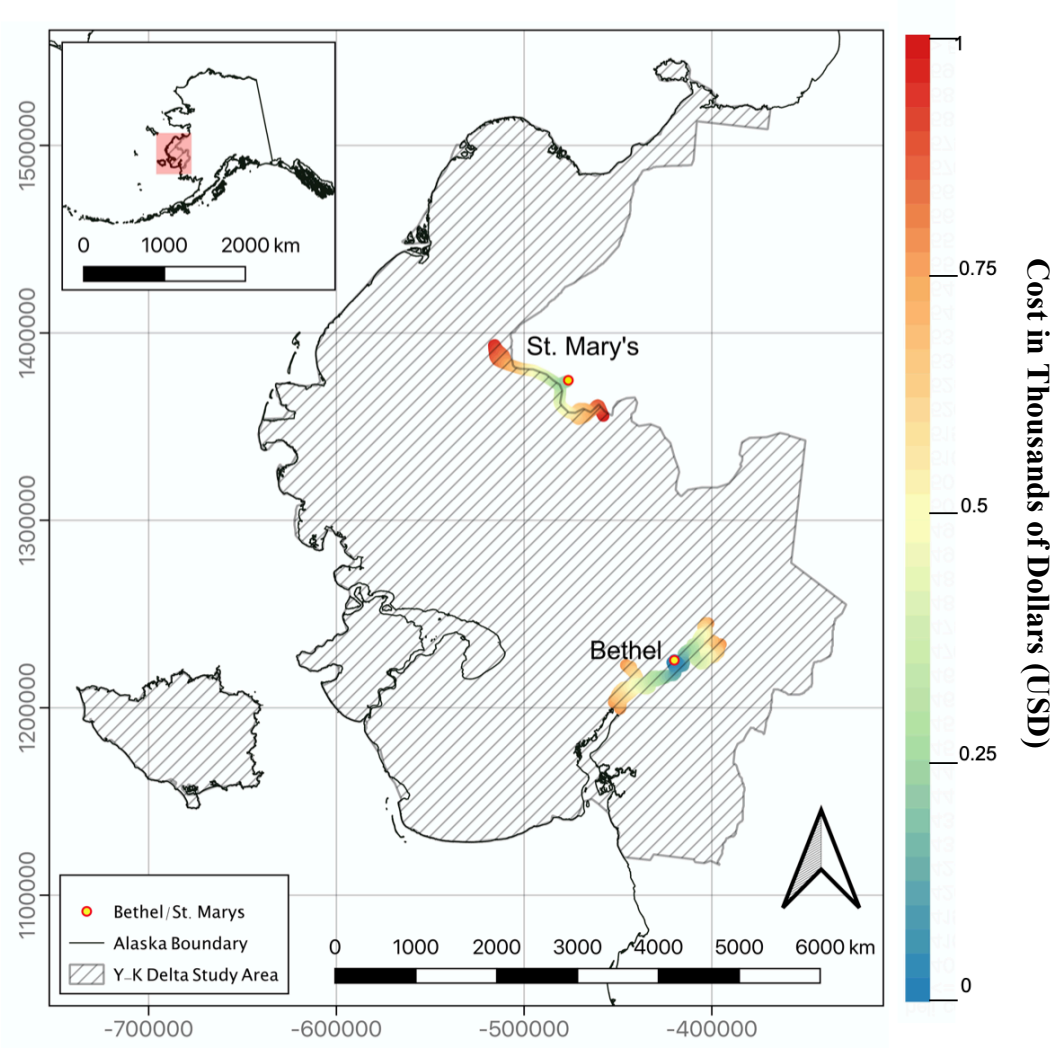

Figure 11. Costs associated with travel by river boat (in thousands of dollars (USD)) in the Yukon-Kuskokwim Delta (Y-K Delta) study area (south western Alaska, inset). Costs are modelled up and downstream for 30 river miles when launched on the Kuskokwim River (Bethel, Alaska) and up and downstream for 30 miles when launched on the Yukon River (St. Mary's, Alaska). Figure creation performed in QGIS version 3.14 (QGIS Development Team, 2020).

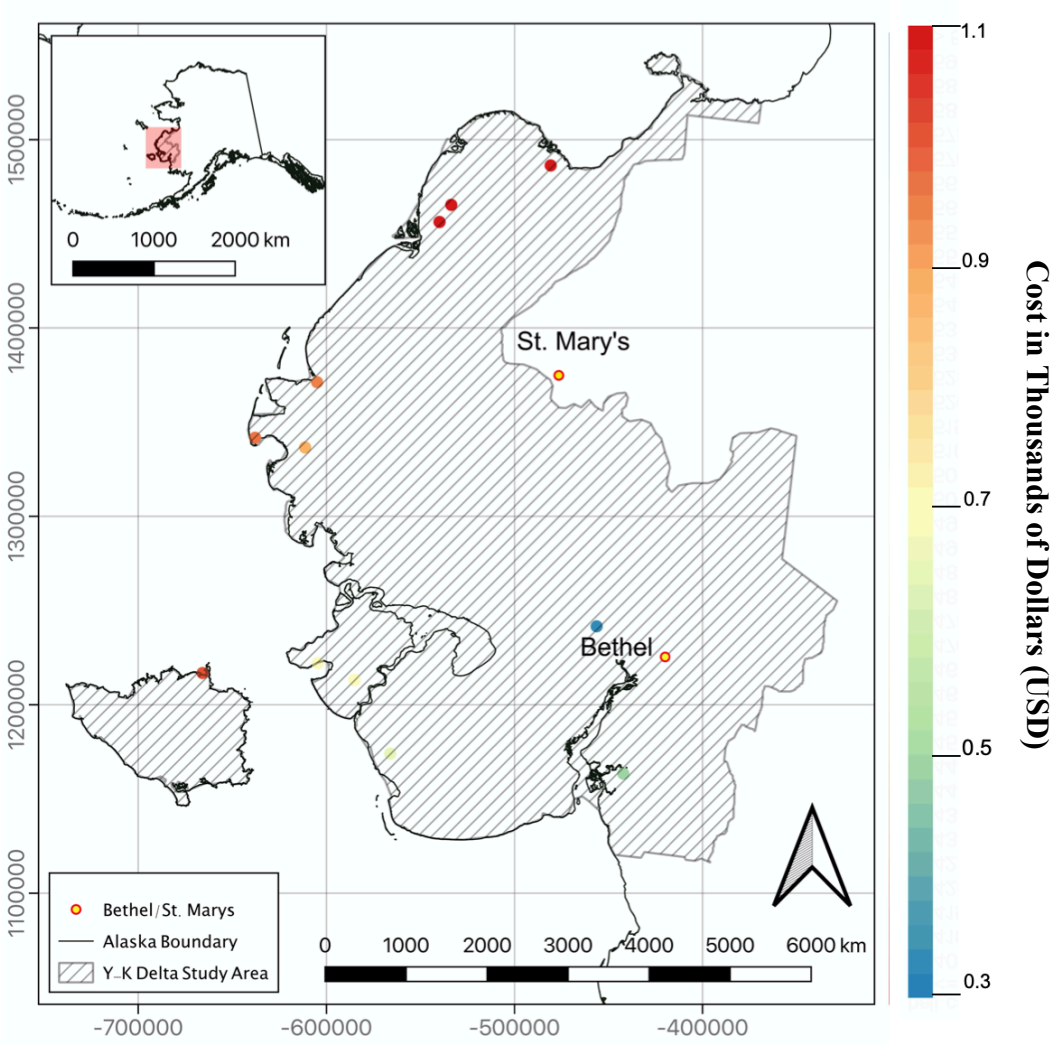

Figure 12. Costs associated with commercial travel and on-foot soil sampling procedures (in thousands of dollars (USD)) for villages contained within the Yukon-Kuskokwim Delta (Y-K Delta) study area (south western Alaska, inset). Figure creation performed in QGIS version 3.14 (QGIS Development Team, 2020).

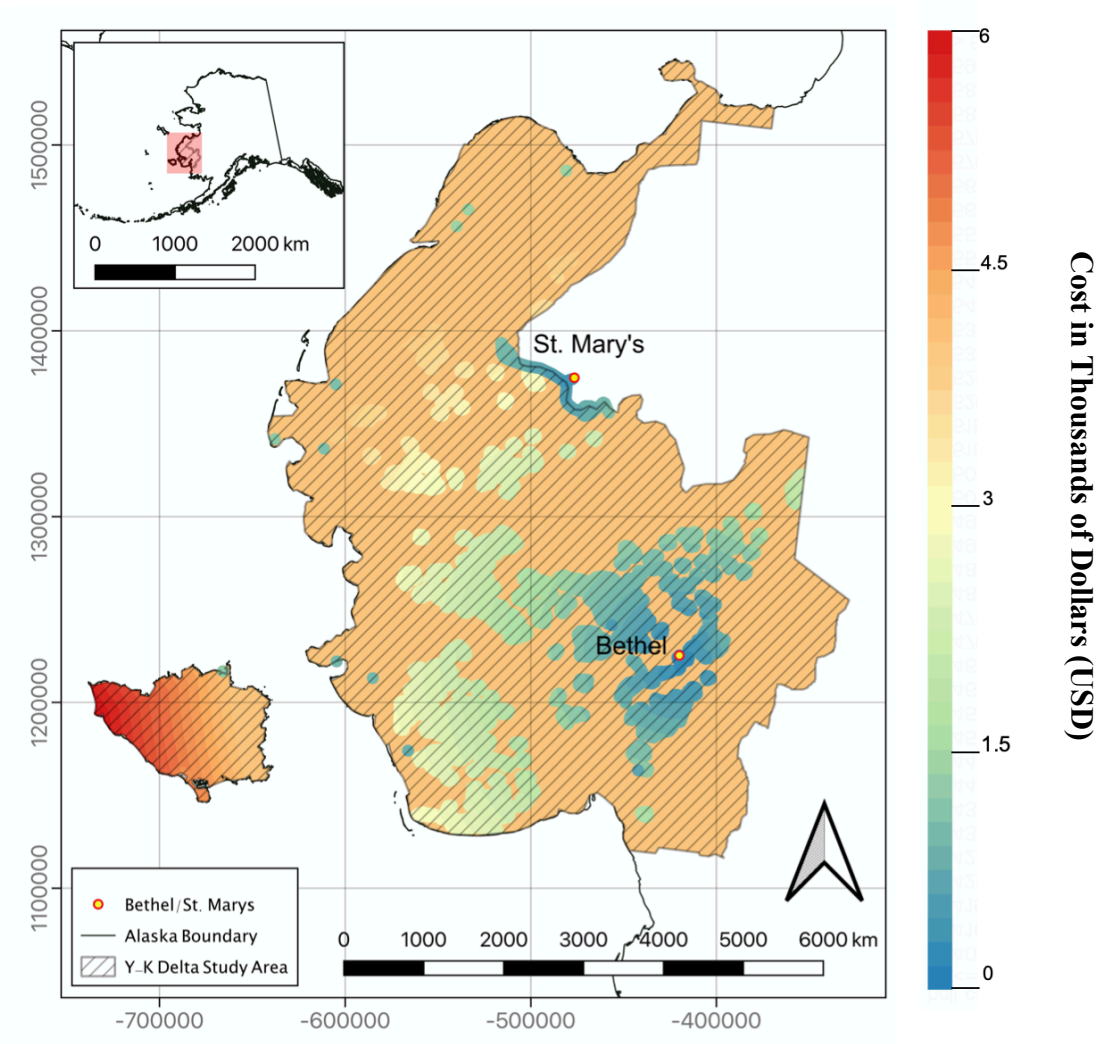

Figure 13. Inclusive, multi-modal cost raster including costs (in thousands of dollars (USD)) associated with travel within the Yukon-Kuskokwim Delta (Y-K Delta) study area in (south western Alaska, inset) Costs are modelled travel by helicopter, float plane, river boat, and on-foot soil sampling methods. Figure creation performed in QGIS version 3.14 (QGIS Development Team, 2020).

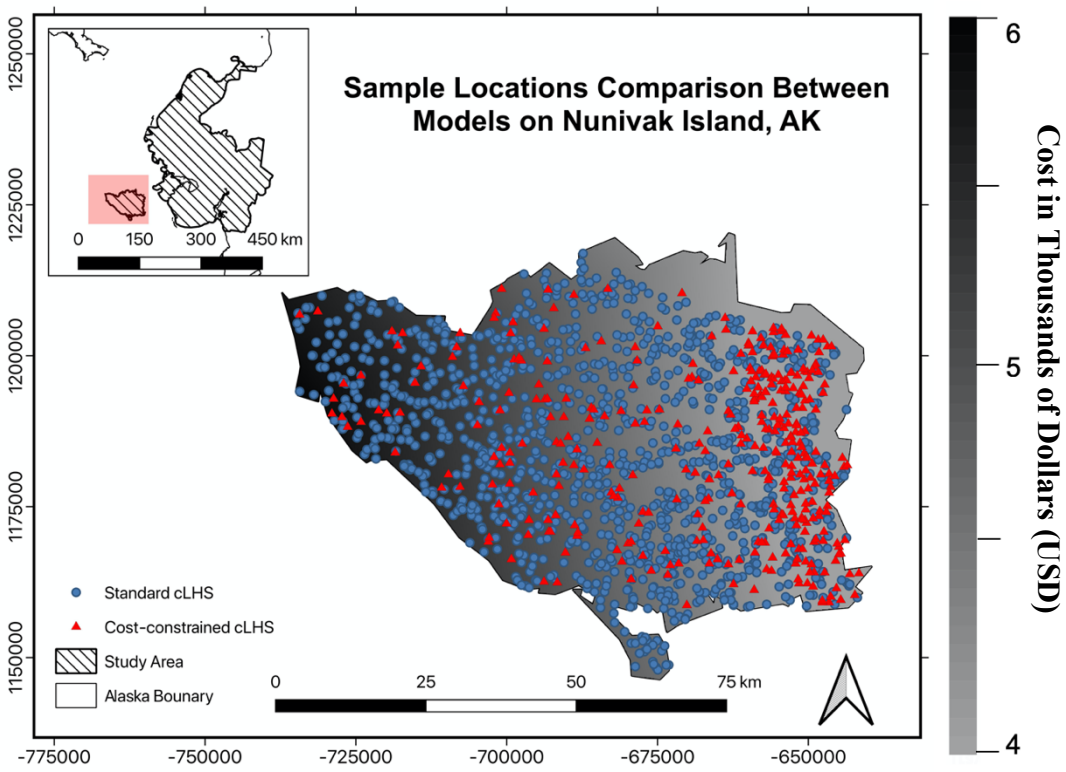

Figure 14. Comparison of the sampling locations given by the standard cLHS
(blue circles) and the cost-constrained cLHS model (red triangles) over 100 re
of each model plotted over a greyscale cost raster illustrating cost of travel to each location in thousands of dollars (USD). Figure creation performed in QGIS version 3.14 (QGIS Development Team, 2020).

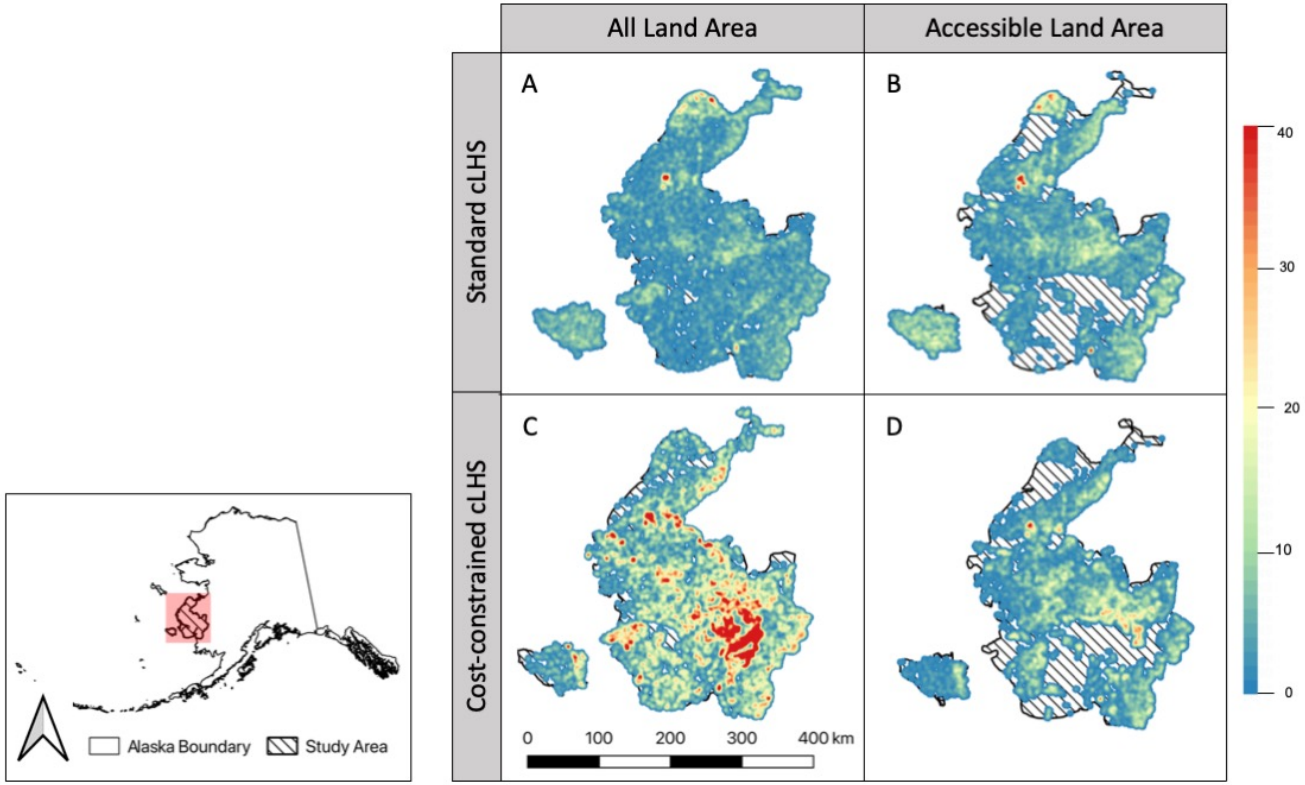

Figure 15. A map of the Yukon-Kuskokwim Delta showing the density of sampling point per 5000m search radius suggested over 100 realizations of the standard cLHS model (including the entire land area (A) and areas that are accessible (B)), and the cost-constrained cLHS model (including the entire land area (C) and areas that are accessible (D)).

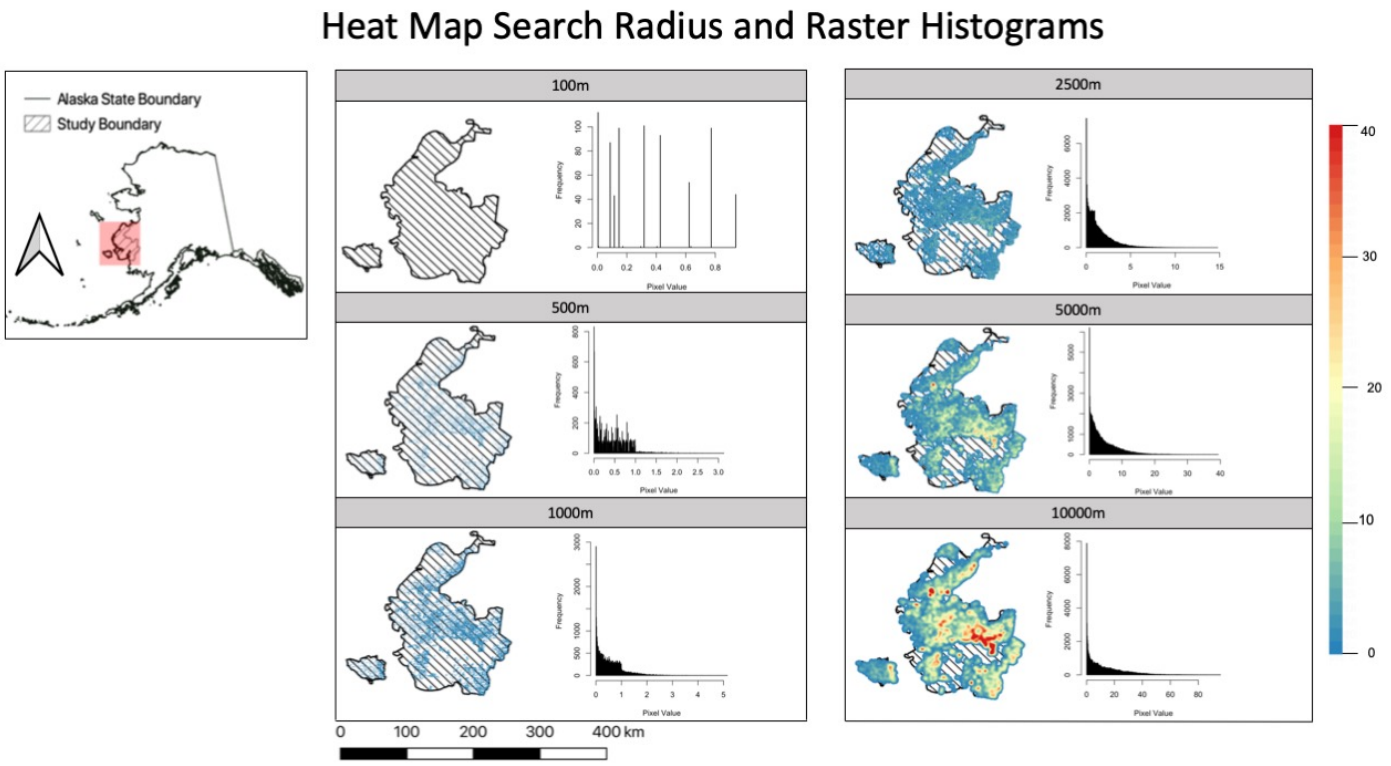

Figure 16. Relationship between cost-constrained cLHS selected sample point density and kernel density (heat maps) with a search radius of 100 m (a), 500 m (b), 1000 m (c), 2500 m (d), 5000 m (e), and 10000 m (f). Histograms displayed with each heat map represent point densities vs. frequency. Relationships are shown for model runs excluding areas designated as off-limits.

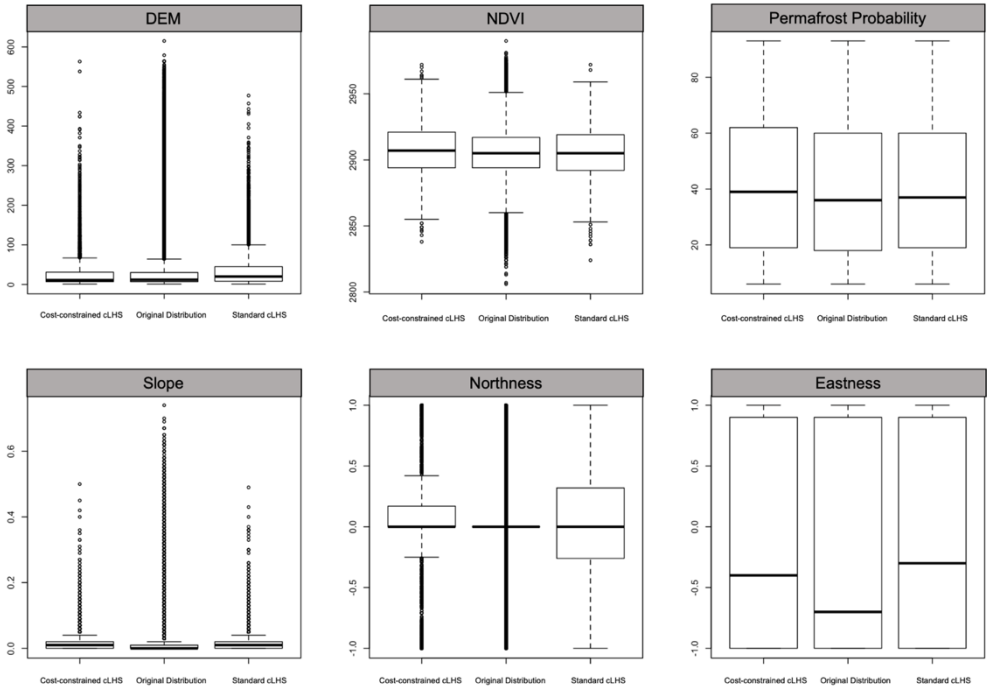

Figure 17. Boxplots comparing differences in environmental covariate feature space distribution coverage by cLHS method for Digital Elevation Model (DEM) (A), Normalized Difference Vegetative Index (NDVI) (B), Permafrost Probability within 1 m (C), Slope (D), Aspect Normalized Northness (E), and Aspect Normalized Eastness (F). Boxplots show original covariate distributions along with distributions of feature space coverage for the standard cLHS model and a cost-constrained cLHS model within the Yukon-Kuskokwim Delta (Y-K Delta) study area. Box plots compare mean and interquartile range (IQR) between environmental covariates for original and model selected distributions. Whiskers on the box plots are 1.5*IQR. Boxplot analysis was performed using input data for accessible areas throughout the Y-K Delta study area.

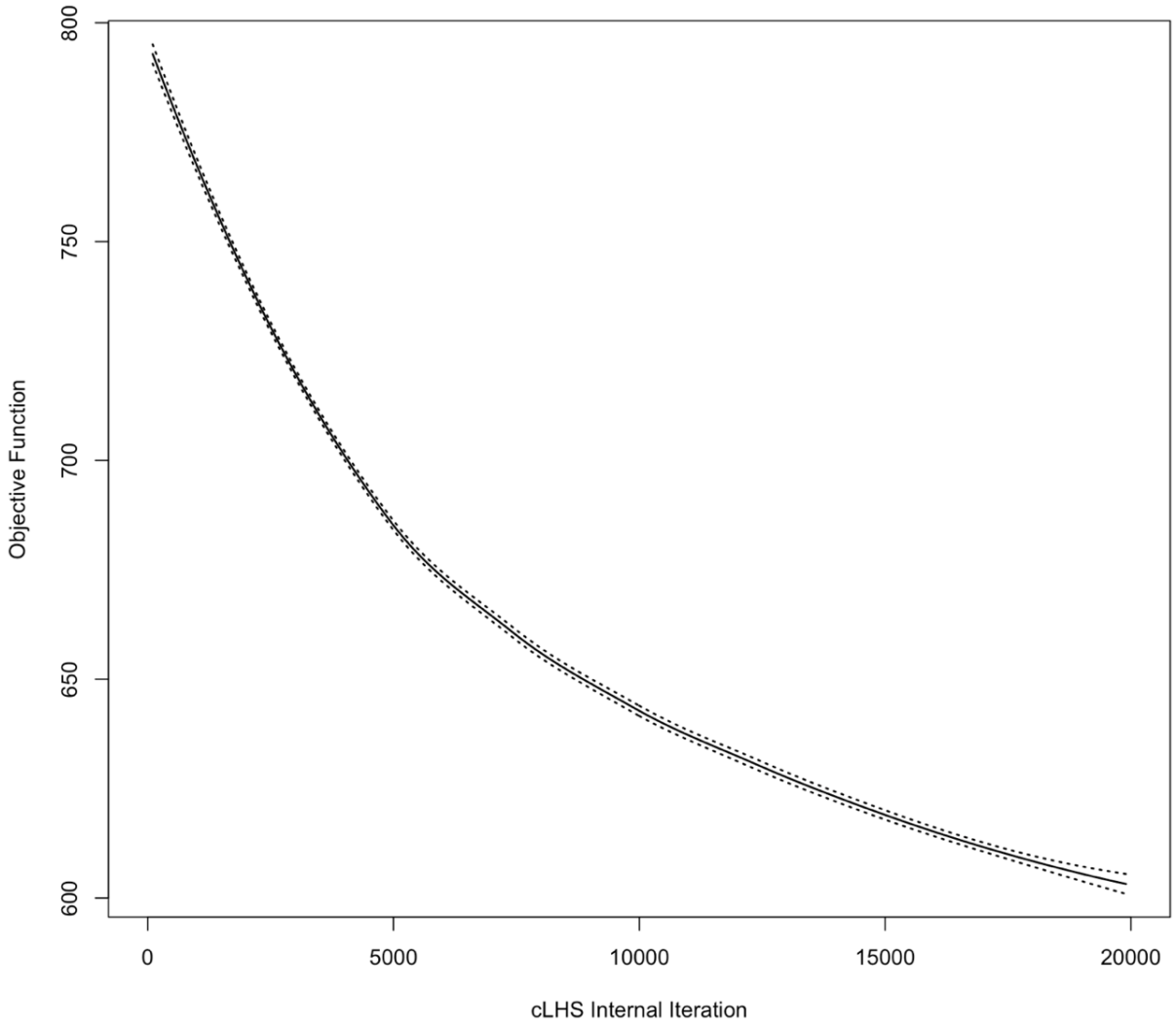

Figure 18. Relationship of the objective function and internal cLHS iteration for the standard cLHS implementation (black) over 10 realizations. Solid line shows a smoothed spline fit to data, while dashed lines show the 95% confidence interval.

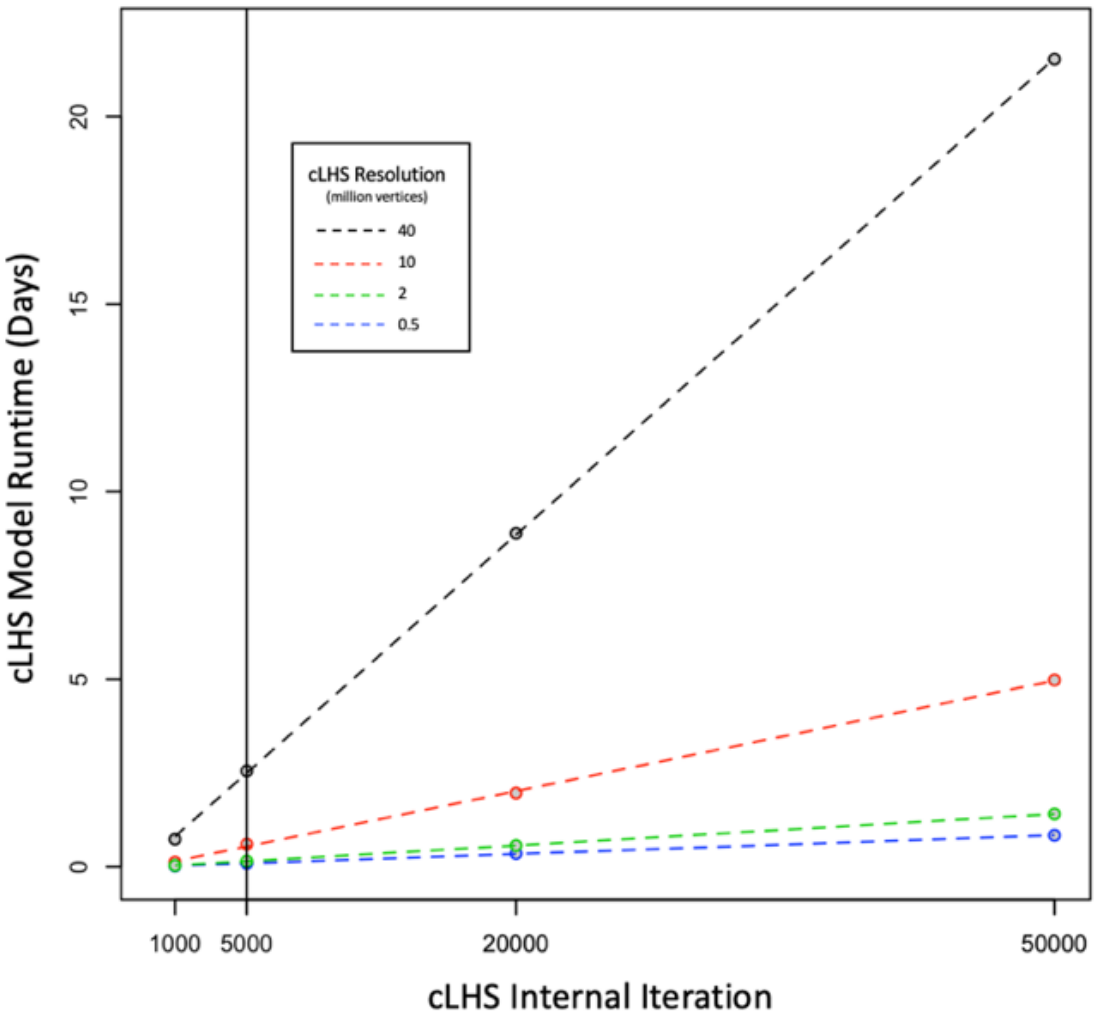

Figure 19. Relationships between internal cLHS iteration, cLHS model resolution (vertices used by model), and model runtimes. Runtimes were recorded for model resolutions of 40 million vertices (black), 10 million vertices (red), 2 million vertices (green), and 0.5 million vertices (blue). Additionally, runtimes were also recorded by subsets of internal cLHS iteration (1000, 5000, 20000, 50000)

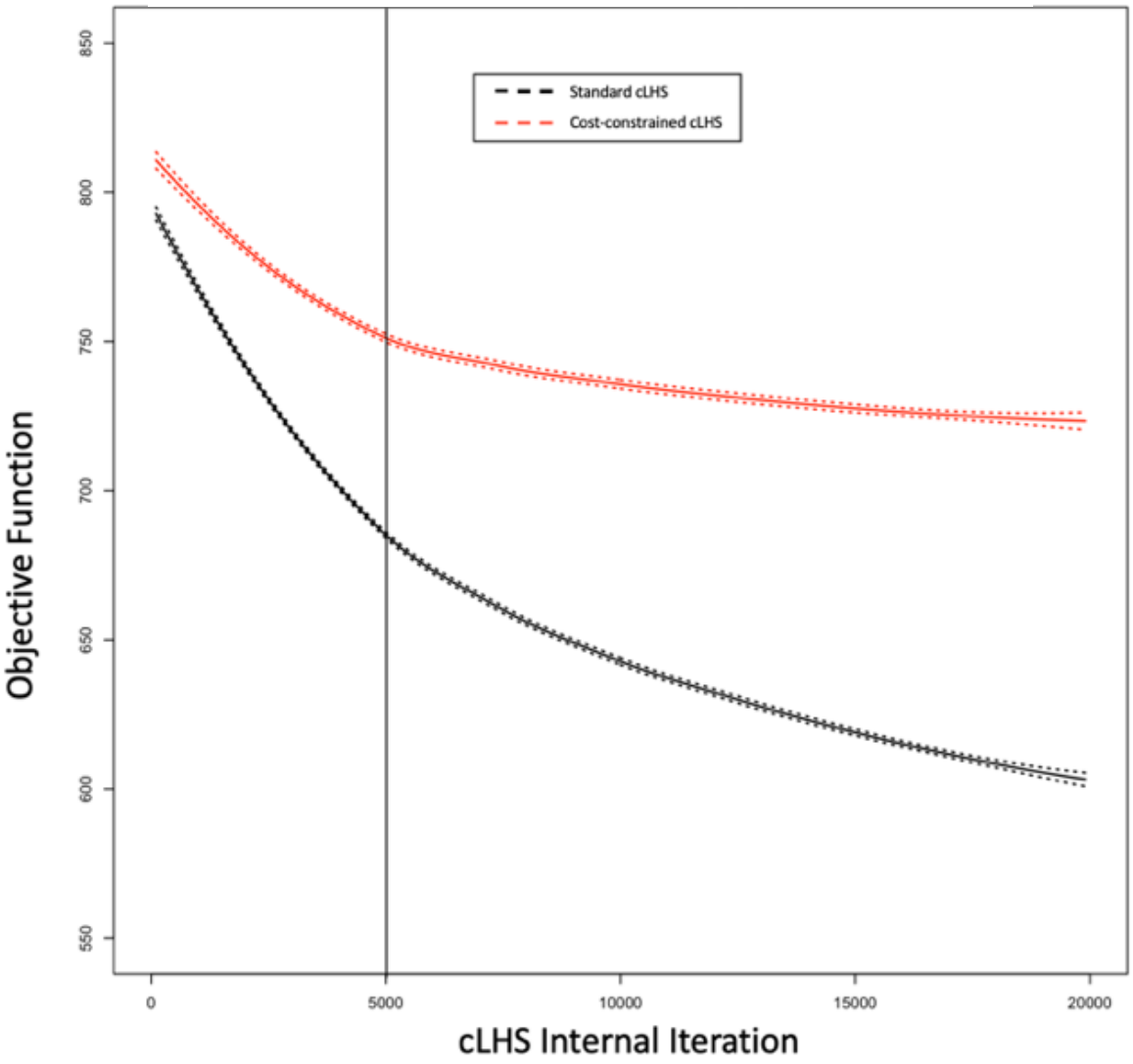

Figure 20. Comparison of the evolution of the objective function for the standard cLHS implementation (black) and the cost-constrained cLHS implementation (red), over 10 realizations. Solid line shows a smoothed spline fit to data, while dashed lines show the 95% confidence interval over 10 realizations.

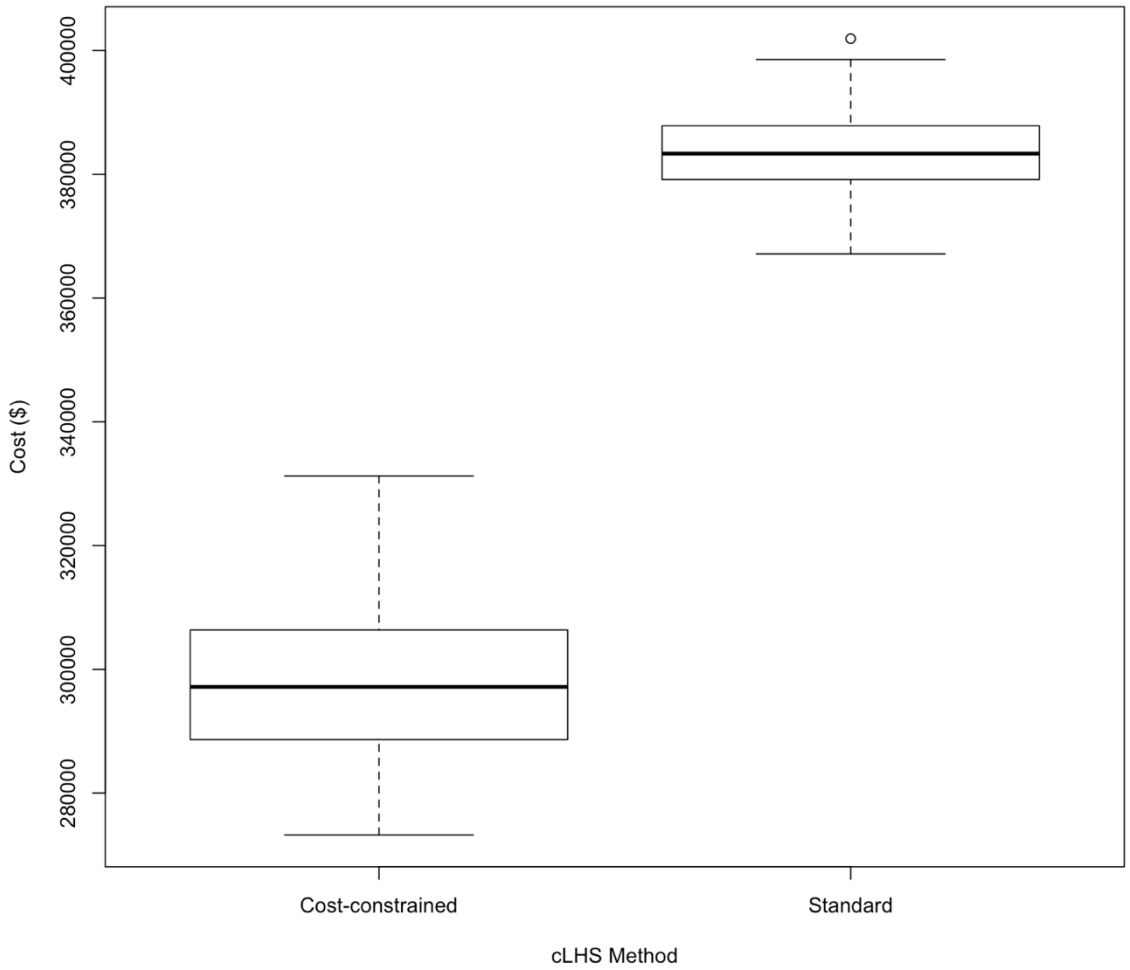

Figure 21. Boxplots comparing the difference in total costs (in US dollars) associated with traveling to field soil sampling locations throughout the Yukon-Kuskokwim Delta, Alaska for cost-constrained and standard cLHS methods. Box plots compare mean and inter-quartile range (IQR) between different models and total costs. Whiskers on the box plots are 1.5xIQR. Costs were calculated by combining data over 100 model realizations.

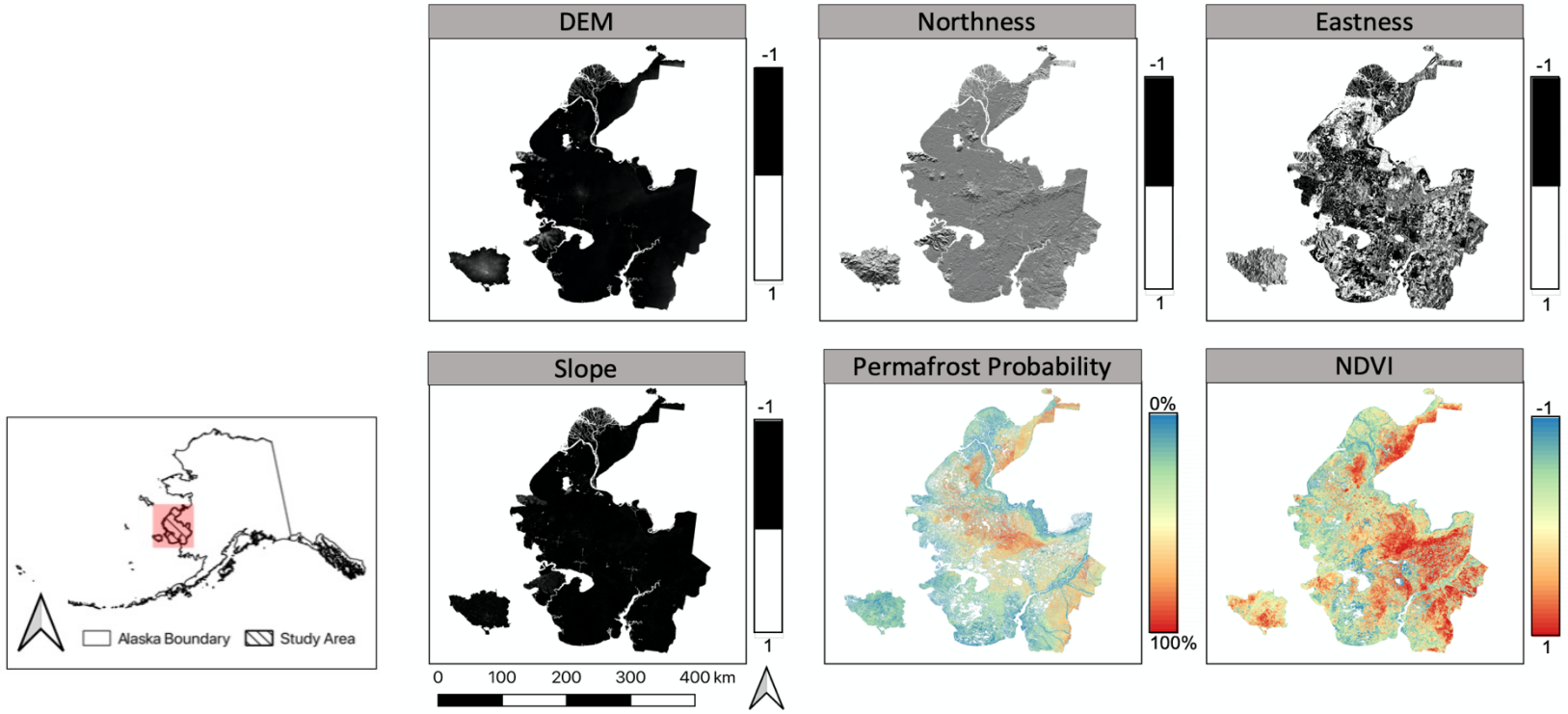

Figure 22. . Environmental covariate raster coverage of the Yukon-Kuskokwim Delta study area for DEM (A), aspect normalized "northness" (B) and "eastness" (C), slope (D), permafrost probability (E), and NDVI (F). All covariates processed in QGIS version 3.14 (QGIS Development Team, 2020).

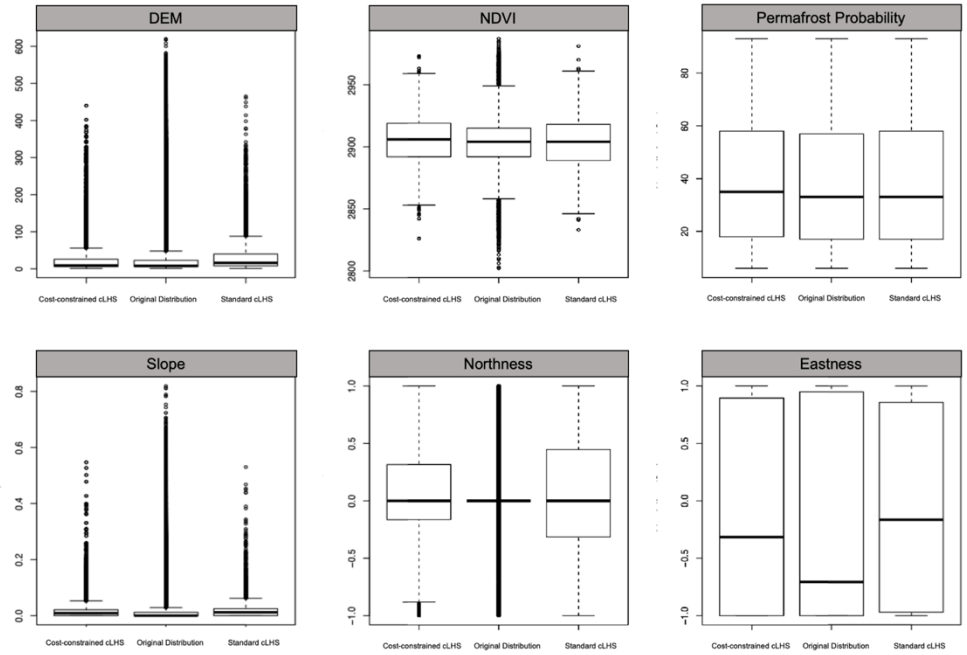

Figure 23. Boxplots comparing differences in environmental covariate feature space distribution coverage by cLHS method for Digital Elevation Model (DEM) (A), Normalized Difference Vegetative Index (NDVI) (B), Permafrost Probability within 1 m (C), Slope (D), Aspect Normalized Northness (E), and Aspect Normalized Eastness (F). Boxplots show original covariate distributions along with distributions of feature space coverage for the standard cLHS model and a cost-constrained cLHS model within the Yukon-Kuskokwim Delta (Y-K Delta) study area. Box plots compare mean and interquartile range (IQR) between environmental covariates for original and model selected distributions. Whiskers on the box plots are 1.5*IQR. Boxplot analysis was performed using input data for all land areas throughout the Y-K Delta study area.

LITERATURE CITED

Alaska Land Use Council. 1984. Susitna joint venture document 2447-III: Fire management information. Alaska Power Authority, Anchorage. www.arlis.org/docs/vol2/hydropower/APA_DOC_no._2446.pdf (accessed 1 Sept. 2019).

Alaska Land Use Council. 1984. Susitna joint venture document 2447-III: Fire management information. Alaska Power Authority, Anchorage. www.arlis.org/docs/vol2/hydropower/APA_DOC_no._2446.pdf (accessed 1 Sept. 2019).

Alaska Interagency Coordination Center (AICC). 2018. Alaska large fires database. https://fire.ak.blm.gov/predsvcs/maps.php (accessed 1 Sept. 2019).

Archontoulis, S.V., and F.E. Miguez. 2015. Nonlinear regression models and applications in agricultural research. Agronomy Journal 107: 786-798.

Beaudette, D.E., Roudier, P., and O'Geen, O.T. 2013. Algorithms for quantitative pedology: A toolkit for soil scientists. Comput. Geosci. 52: 258–268. doi:10.1016/j.cageo.2012.10.020

Bennett, M.R., Huddart, D., and Thomas, G.S.P. 2012. Facies architecture within a regional glaciolacustrine basin: Copper River, Alaska. Quat. Sci. Rev. 21:2237–2279. doi:10.1016/S0277-3791(02)00027-6

Bhatti, J.S., and Apps, M.J. 2000. Carbon and nitrogen storage in upland boreal forests. In Global climate change and cold regions ecosystems. Edited by R. Lal, J.M. Kimble, and B.A. Stewart. CRC Press, Boca Raton, Fla. pp. 79–90.

Bhatti, J.S., Apps, M.J., Jiang, H., 2002. Influence of nutrients, disturbances and site conditions on carbon stocks along a boreal forest transect in central Canada. Plant and Soil. 242, 1–14. https://doi.org/10.1023/A:1019670619316

Clark, M.H., and Kautz, D.R. 1990. Soil survey of Copper River area, Alaska. USDA–NRCS, Washington, DC.

Clark, M.H., and Kautz, D.R. 1999. Soil and Vegetation Survey of the Gulkana River Area, Alaska. BLM-Alaska Technical Report 20. U.S. Department of the Interior, Bureau of Land Management, Alaska State Office, Anchorage, AK.

Collins, M., Knutt, R., Arblaster, J., Dufresne, J.L., Fichefet, T., Friedlingstein, P., 2013. Long-term climate change: Projections, commitments and irreversibility. In: Stocker, T.F., Qin, D., Plattner, G.K., Tignor, M., Allen, S.K., Boschung, J., Nauels, A., Xia, Y., Bex, V., and Midgley, P.M., (editors), 2013. The physical science basis. Contribution of working group I to the fifth assessment report of the intergovernmental panel on climate change. Clim. Chan. Cambridge Univ. Press, Cambridge, UK and New York. 1029–1136.

Dyrness, C.T. 1982. Control of depth to permafrost and soil temperature by the forest flow in black spruce/feathermoss communities. Research Note PNW-396, United States Department of Agriculture, Forest Service. Pacific Northwest Forest and Range Experiment Station. Portland, OR.

Dyrness, C.T., and Norum, R.A. 1983. The effects of experimental fires on black spruce forest floors in interior Alaska. Can. Jour. For. Res. 13: 879-893.

Ferrians, O.J. 1983. Pleistocene glacial history of the northeastern Copper River Basin, Alaska. GSA Abstracts Programs 16(5): 282.

Fisher, J.P., Estop-Aragonesm, C., Thierry A., Charman, D.J., Wolfe, S.A., Hartley, I.P. 2016. The influence of vegetation and soil characteristics on active-layer thickness of permafrost soils in boreal forest. Glob. Chan. Biol. 22: 3127–3140. doi:10.1111/gcb.13248

Franklin, J.F., Spies, T.A., Pelt, R.V., Carey, A.B., Thornburgh, D.A., Berg, D.R., Chen, J. 2002. Disturbances and structural development of natural forest ecosystems with silvicultural implications, using Douglas-fir forests as an example. For. Eco. Manag. 155(1-3): 399–423. doi: 10.1016/s0378-1127(01)00575-8

Fryer, J.L. 2014. Fire regimes of Alaskan black spruce communities. USDA Forest Service, Rocky Mountains Research Station, Fire Sciences Laboratory. www.fs.fed.us/database/feis/fire_regimes/AK_black_spruce/all.html (accessed 7 Sept. 2019).

Gesch, D., Oimoen, M., Greenlee, S., Nelson, C., Steuck, M., & Tyler, D. 2002. The national elevation dataset. Photogrammetric Engineering and Remote Sensing, 68, 5–11.

Gallant, A.L., E.F. Binnian, J.M. Omernik, and M.B. Shasby. 1995. Ecoregions of Alaska. USGS, Denver, CO

Genet, H., McGuire, A.D., Barrett, K., Breen, A., Euskirchen, E.S., and Johnstone, J.F. 2013. Modeling the effects of fire severity and climate warming on active layer thickness and soil carbon storage of black spruce forests across the landscape in interior Alaska. Environ. Res. Lett. 8(4): 45-56. doi:10.1088/1748-9326/8/4/045016

Heinselman, M.L. 1981. Fire intensity and frequency as factors in the distribution and structure of northern ecosystems. Pages 7-57 in Mooney H. A., Bonnicksen T. M., Christensen N. L., Lottan J. E., and Reiners W. A., editors. Fire Regimes and Ecosystem Processes, General Technical Report WO-26. USDA Forest Service, Washington, DC.

Hewitt, A., McKenzie, N., Grundy, M., Slater, B. Qualitative survey. McKenzie, N.J., Grundy, M.J., Webster, R., and Ringrose-Voase, A.J. Guidelines for Surveying Soil and Land Resources, Australian Soil and Land Survey Handbook Series, CSIRO Publishing, Canberra. 2008, pp. 285-306

Hinton, R. B., Girdner, C. L., United States, & Soil Conservation Service. 1966. Soils of the Bethel area, Alaska. Soil Conservation Service.

Hollingsworth, T.N. 2004. Quantifying variability in the Alaskan black spruce ecosystem: Linking vegetation, carbon, and fire history. Ph.D. diss., Univ. of Alaska-Fairbanks, Fairbanks.

Hoy, E.E., Turetsky, M.R., and Kasischke, E.S. 2016. More frequent burning increases vulnerability of Alaskan boreal black spruce forests. Environ. Res. Lett. 11:095001. doi:10.1088/1748-9326/11/9/095001

Howell, D., Kim, Y., Haydu-Houdeshell, C., Clemmer, P., Almaraz, R., and Ballmer, R. 2006. Fitting soil property spatial distribution models in the Mojave Desert for digital soil mapping. p. 465-475. In: Lagacherie, P., McBratney, A.B., and Voltz, M. Digital Soil Mapping: An introductory perspective. Developments in Soil Science Vol. 31, Elsevier, Amsterdam

Hu, F. S., Brubaker, L.B., Gavin, D.G., Higuera, P.E., Lynch, J.A., Rupp T.S., and Tinner, W. 2006. How Climate and Vegetation Influence the fire Regime of the Alaskan Boreal Biome: The Holocene Perspective. Mitigation and Adaptation Strategies for Global Change, 11(4): 829–846. doi: 10.1007/s11027-005-9015-4

Iman, R.L., Helton, J.C., and Campbell, J.E., 1981. An approach to sensitivity analysis of computer models, Part 1. Introduction input variable selection and preliminary variable assessment. Journal of Quality Technology. 13 (3) pg. 174–183. doi:10.1080/00224065.1981.11978748

Jelinski, N.A., Sousa, M.J., Williams, A., Greybear, E., Finnesand, K., Mulligan, D., and Feinberg, J.M. 2019. Cryoturbation and Carbon Stocks in Gelisols under Late-Successional Black Spruce Forests of the Copper River Basin, Alaska. Soil Sci. Soc. Am. Jour., 83(6): 1760–1778. doi: 10.2136/sssaj2019.07.0212

Jennings, M., D. Faber-Langendoen, R. Peet, O. Loucks, D. Glenn-Lewin, A. Damman, M. Barbour, et al. 2004. Guidelines for describing associations and alliances of the U.S. national vegetation classification, version 4.0. Vegetation Classification Panel. Washington D.C.: The Ecological Society of America.

Johnson, E.A. 1979. Fire recurrence in the subarctic and its implications for vegetation composition. Canadian Journal of Botany, 57(12): 1374–1379. doi: 10.1139/b79-171

Johnson, K.D., Harden, J., McGuire, A.D., Bliss, N.B., Bockheim,, J.G., and Clark, M.H. 2011. Soil carbon distribution in Alaska in relation to soil-forming factors. Geoderma 167-168; 71–84. doi:10.1016/j.geoderma.2011.10.006

Jorgenson, M. T., and Osterkamp, T. E. 2005. Response of boreal ecosystems to varying modes of permafrost degradation. Can. Jour. For. Res., 35(9): 2100–2111. doi: 10.1139/x05-153

Kane, E. S. 2006. Mechanisms of soil carbon stabilization in black spruce forests of interior Alaska: Soil temperature, soil water, and wildfire.

Kasischke, E.S., O'Neill K. P., French N.H.F., and Bourgeau-Chavez, L.L. 2000. Controls on patterns of biomass burning in Alaskan boreal forests. Pages 173-196 in Kasischke E.S. and Stocks B.J., editors. Fire, Climate Change, and Carbon Cycling in the North American Boreal Forest. Springer-Verlag, New York.

Kasischke, E.S., and Johnstone, J. F. 2005. Variation in postfire organic layer thickness in a black spruce forest complex in interior Alaska and its effects on soil temperature and moisture. Can. Jour. For. Res., 35(9): 2164–2177. doi: 10.1139/x05-159

Kasischke, E.S., and Turetsky, M.R. 2006. Recent changes in the fire regime across the North American boreal region—Spatial and temporal patterns of burning across Canada and Alaska. Geophysi. Res. Lett., 33(9), doi: 10.1029/2006gl025677

Kasischke, E.S., David V.L., Rupp, T., Scott, M.A. David, M., Karen A., Jandt, R.B, Jennifer L.H., Elizabeth E.D., Paul A.C., Monika, T.R. 2010. Alaska's changing fire regime--implications for the vulnerability of its boreal forests. Can. Jour. For. Res. 40: 1313-1324.

Knudson, K.J., Frink, L., Hoffman, B.W., and Price, T.D. 2004. Chemical characterization of Arctic soils: Activity area analysis in contemporary Yup'ik fish camps using ICP-AES. Journal of Archaeological Science, 31(4), pg. 443–456. https://doi.org/10.1016/j.jas.2003.09.011

LANDFIRE. 2017. LANDFIRE biophysical settings layer: LF 2014– LF 1.4.0. US Department of Interior, Geological Survey. www.landfire.gov/lf_140.php (accessed 29 Mar. 2019).

Landhausser, S.M., and Wein, R.W. 1993. Postfire Vegetation Recovery and Tree Establishment at the Arctic Tree line: Climate-Change-Vegetation-Response Hypotheses. The Journal of Ecology, 81(4): 665. doi: 10.2307/2261664

Lynch, J.A., Hollis, J.L., and Hu, F.S. 2004. Climatic and landscape controls of the boreal forest fire regime: Holocene records from Alaska. Jour. of Ecol. 92(3): 477-489.

Metropolis, N., Rosenbluth, A.W., Rosenbluth, M.N., Teller, A.H., and Teller, E. 1953. Equation of State Calculations by Fast Computing Machines. Journal of Chemical Physics 21, pg. 1087–1092

McKay, M.D., Beckman, R.J., and Conover, W.J. 1979. A Comparison of Three Methods for Selecting Values of Input Variables in the Analysis of Output from a Computer Code. Technometrics. American Statistical Association. 21 (2): pg. 239- 245. doi:10.2307/1268522

McKenzie, N.J. and Ryan, P.J. 1999. Spatial prediction of soil properties using environmental correlation. Geoderma 89(1-2): pg. 67-94

Minasny, B., and McBratney, A.B. 2006. A conditioned Latin hypercube method for sampling in the presence of ancillary information. Computers & Geosciences, 32(9), pg. 1378–1388. https://doi.org/10.1016/j.cageo.2005.12.009

Michaelson, G.J., Ping, C.L., and Kimble, J.M. 1996. Carbon content and distribution in tundra soils in arctic Alaska, U.S.A, Arct. Alp. Res., 28: 414 – 424.

Minsley, B.J., Pastick, N.J., Wylie, B.K., Brown, D.R.N., and Kass, M. 2016. Evidence for nonuniform permafrost degradation after fire in boreal landscapes. Jour. Geophys. Res. Earth Surf. 121, 320–335. doi:10.1002/2015JF003781

Miyanishi, K., and Johnson, E.A. 2003. Process and patterns of duff consumption in the mixwood boreal forest. Can. Jour. For. Res. 32: 1285-1295.

Muhs, D.R., Budahn, J. R., McGeehin, J.P., Bettis, E.A., Skipp, G., Paces, J.B., and Wheeler, E.A. 2013. Loess origin, transport, and deposition over the past 10,000years, Wrangell-St. Elias National Park, Alaska. Aeolian Research 11: 85-99. https://doi.org/10.1016/j.aeolia.2013.06.001.

Mulder, V.L., de Bruin, S., and Schaepman, M.E. 2012. Representing major soil variability at regional scale by constrained Latin Hypercube Sampling of remote sensing data. International Journal of Applied Earth Observation and Geoinformation

Nowacki, G., Spencer, P., Brock, T., Fleming, M., & Jorgenson, M.T. 2001. Ecoregions of Alaska and neighboring territory. U.S. Geological Survey, Reston, VA. Open File Report 2002-297. https://databasin.org/maps/c1ff699cdb624d2399c21236a9b65228

O'Donnell, J.A., Romanovsky, V.E., Harden, J.W., and McGuire, A.D. 2009. The effect of moisture content on the thermal conductivity of moss and organic soil horizons from black spruce ecosystems in interior Alaska. Soil Sci. 174(12): 646–651. doi:10.1097/SS.0b013e3181c4a7f8

O'Donnell, J.A. 2010. The effects of permafrost degradation on soil carbon in Alaska's Boreal Region. PhD Dissertation, University of Alaska-Fairbanks.

O'Donnell, J.A., Harden, J.W., McGuire, A.D., Kanevskiy, M.Z., Jorsenson, M.T., and Xu, X.O. 2011. The effect of fire and permafrost interactions on soil carbon accumulation in an upland black spruce ecosystem of interior Alaska: Implications for post-thaw carbon loss. Glob. Change Biol. 17: 1461–1474. doi:10.1111/j.1365-2486.2010.02358.x

Oliver, C.D., and Larson, B.L. 1996. Forest stand dynamics. New York, NY: Wiley.

Pastick, N.J., Jorgenson, M.T., Wylie, B.K., Nield, S.J., Johnson, K.D., and Finley, A.O. 2015. Distribution of near-surface permafrost in Alaska: Estimates of present and future conditions. Rem. Sens. Environ. 168: 301-315. doi: 10.1016/j.res.2015.07.019

Pastick, N. J., Duffy, P., Genet, H., Rupp, T.S., Wylie, B.K., and Johnson, K.D. 2017. Historical and projected trends in land- scape drivers affecting carbon dynamics in Alaska. Ecological Applications, 27(5), 1383–1402. https://doi.org/10.1002/eap.1538

Pastick, N.J., Jorgenson, M.T., Goetz, S.J., Jones, B.M., Wylie, B.K., Minsley, B.J., Genet, H., Knight, J.F., Swanson, D.K., and Jorgenson, J.C. 2019. Spatiotemporal remote sensing of ecosystem change and causation across Alaska. Glob. Chan. Bio. 25: 1171-1189.

Pettitt, A.N., and McBratney, A.B. 1993. Sampling Designs for Estimating Spatial Variance Components. Journal of the Royal Statistical Society: Series C (Applied Statistics), 42(1), pg. 185–209. https://doi.org/10.2307/2347420

Ping, C.-L., Clark, M.H., and Swanson, D.K. 2004. Cryosols in Alaska. In: J.M. Kimble, editor, Cryosols. Springer-Verlag, Heidelberg, Germany. p. 71-94 doi:10.1007/978-3-662-06429-0_5

Ping, C.-L., G.J. Michaelson, E.S. Kane, E.C. Packee, C.A. Stiles, D.K. Swanson, and N.D. Zaman. 2010. Carbon stores and biogeochemical properties of soils under black spruce forest, Alaska. Soil Science Society of America Journal 74(3): 969-978.

Ping, C. L., Clark, M.H., Kimble, J.M., Michaelson, G.J., Shur, Y., and Stiles, C.A. 2013. Sampling protocols for permafrost-affected soils. Soil Horiz. 54: 13–19.

Porter, C., et al., 2018, "ArcticDEM", https://doi.org/10.7910/DVN/OHHUKH, Harvard Dataverse, V1, Accessed 1 Jan, 2020.

QGIS Development Team, 2020. QGIS Geographic Information System. Open Source Geospatial Foundation Project. http://qgis.osgeo.org

R Core Team. 2016. R: A language and environment for statistical computing. R Foundation for Statistical Computing, Vienna, Austria.

Rand, J., and M. Mellor. 1985. Ice-coring augers for shallow depth sampling. CRREL Report 85-21. U.S. Army Corps of Engineers Cold Regions Research & Engineering Laboratory, Hanover, NH https://apps.dtic.mil/dtic/tr/fulltext/u2/a166630.pdf (accessed 7 Sept. 2019).

Ravn Alaska. 2020. *Book Flights*. Retrieved from https://ravnalaska.com

Rosner, C. 2004. Growth and Yield of Black Spruce, Picea mariana (Mill.) BS Pl., in Alaska (Doctoral dissertation, University of Alaska Fairbanks, School of Natural Resources and Agricultural Sciences). https://rb.gy/7ykak7

Roudier, P. 2011. clhs: a R package for conditioned Latin hypercube sampling. http://cran.r- project.org/web/packages/clhs/index.html

Roudier, P., Beaudette, D., and Hewitt, A. 2012. A conditioned Latin hypercube sampling algorithm incorporating operational constraints pg. 227–232. https://doi.org/10.1201/b12728-46

Scarpone, C., Schmidt, M.G., Bulmer, C.E., and Knudby, A. 2016. Modelling soil thickness in the critical zone for Southern British Columbia. Geoderma, 282, pg. 59–69. https://doi.org/10.1016/j.geoderma.2016.07.012

Schoeneberger, P.J., Wysocki, D.A., and Benham E.C. (editors). 2011. Field book for describing and sampling soils, Version 3.0. Natural Resources Conservation Service, National Soil Survey Center, Lincoln, NE

Sniderhan, A.E., and Baltzer, J.L. 2016. Growth dynamics of black spruce (Picea mariana) in a rapidly thawing discontinuous permafrost peatland. J. Geophys. Res. Biogeosci., 121: 2988-3000. doi: 10.1002/2016JG003528

Soil Classification Working Group 1998. The Canadian System of Soil Classification, 3rd ed. Agriculture and Agri-Food Canada Publication 1646. ISBN 0-660-17404-9.

Soil Survey Staff. 1993. Soil survey manual. Soil Conservation Service. U.S. Department of Agriculture Handbook 18

Soil Survey Staff, Natural Resources Conservation Service U.S. Department of Agriculture. 1995. Soil Survey of Kobuk Preserve Unit and Gates of The Arctic National Park, Alaska. Available online at https://www.nrcs.usda.gov. Accessed [09 Nov 2020]

Soil Survey Staff, Natural Resources Conservation Service U.S. Department of Agriculture. 2005. Soil Survey of Western Interior Rivers Area, Alaska. Available online at https://www.nrcs.usda.gov. Accessed [09 Nov 2020]

Soil Survey Staff, Natural Resources Conservation Service, U.S. Department of Agriculture. 2019. U.S. General Soil Map (STATSGO2). Available online at https://sdmdataaccess.sc.egov.usda.gov. Accessed [09 Nov 2020]

Sun, X.L., Wang, H.L., Zhao, Y.G., Zhang, C., and Zhang, G.L. 2017. Digital soil mapping based on wavelet decomposed components of environmental covariates. Geoderma, 303, 118–132. https://doi.org/10.1016/j.geoderma.2017.05.017

Thorsteinson, L.K., Becker, P.R., and Hale, D.A. 1989. The Yukon Delta: A synthesis of information. Anchorage, AK: NOAA/National Ocean Service, Ocean Assessments Division, Alaska Office

Turetsky, M.R., Kane, E.S., Harden, J.W., Ottmar, R.D., Manies, K.L., Hoy, E., Kasischke, E.S. 2011. Recent acceleration of biomass burning and carbon losses in Alaskan forests and peatlands Nat. Geosci. 4:27–31. doi:10.1038/ngeo1027

U.S. Census Bureau. 2010. Geographic Identifiers: 2010 Demographic Profile Data: Bethel city, Alaska. Retrieved [09 Nov 2020].

Viereck, L.A. 1970. Forest succession and soil development adjacent to the Chena River in interior Alaska. Arc. Alp. Res. 2:1–26.

Viereck, L.A., Dyrness, C.T., Cleve, K.V., and Foote, M. J. 1983a. Vegetation, soils, and forest productivity in selected forest types in interior Alaska. Can. Jour. For. Res., 13(5): 703–720. doi: 10.1139/x83-101

Viereck, L.A. 1983b. The effects of fire in black spruce ecosystems of Alaska and northern Canada. Pages 201-220 in R. Wein, W. and MacLean, D.A. editors. The Role of Fire in Northern Circumpolar Ecosystems. John Wiley & Sons, Chichester.

Webb, E.E., Heard, K., Natali, S.M., Bunn, A.G., Alexander, H.D., and Berner, L.T. 2017. Variability in above- and belowground carbon stocks in a Siberian larch watershed. Biogeo. 14:4279–4294. doi:10.5194/bg-14-4279-2017

Welch, B. L. (1947). "The generalization of "Student's" problem when several different population variances are involved". Biometrika. 34 (1–2): 28–35. doi:10.1093/biomet/34.1-2.28. MR 0019277. PMID 20287819

Yarie, J. 1981. Forest fire cycles and life tables: a case study from interior Alaska. Can. Jour. For. Res. 11:554-562.

Yi, S., Manies, K., Harden, J., and Mcguire, A.D. 2009a. Characteristics of organic soil in black spruce forests: Implications for the application of land surface and ecosystem models in cold regions. Geophy. Res. Let. 36(5). doi: 10.1029/2008gl037014

Yi, S., Mcguire, A.D., Harden, J., Kasischke, E., Manies, K., Hinzman, L., and Kim, Y. 2009b. Interactions between soil thermal and hydrological dynamics in the response of Alaska ecosystems to fire disturbance. Biogeosci. 114(G2). doi: 10.1029/2008jg000841

Zhuang, Q., McGuire, A.D., O'Neill, K.P., Harden, J.W., Romanovsky, V.E. and Yarie, J. 2003. Modeling soil thermal and carbon dynamics of a fire chronosequence in interior Alaska. J. Geophys. Res. 108: FFR 3–1 to 3–26.